Article

Structure

Structural mechanism of HP1α-dependent transcriptional repression and chromatin compaction

Graphical abstract

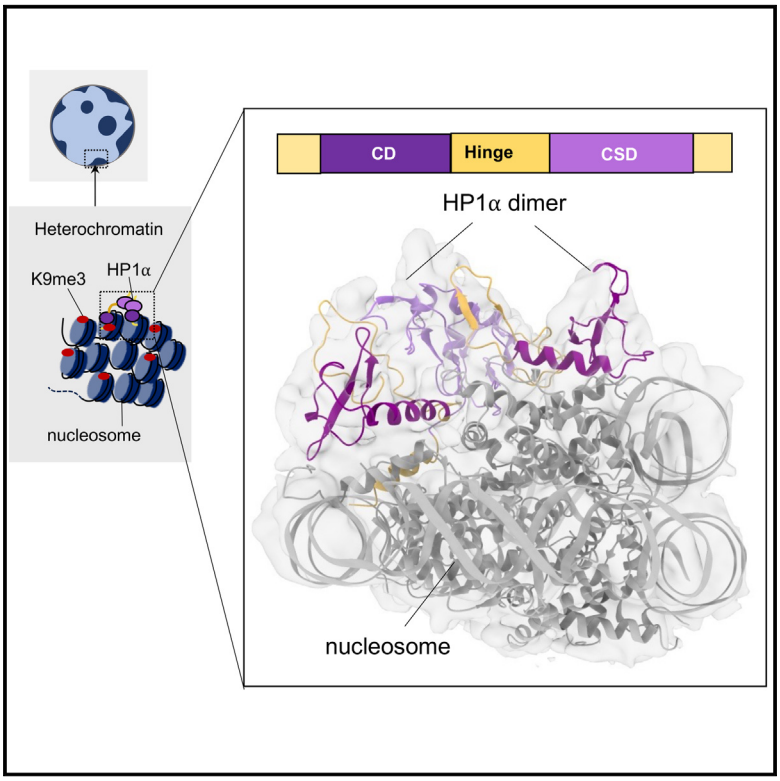

Authors

Vladyslava Sokolova, Jacob Miratsky, Vladimir Svetlov, ..., Evgeny Nudler, Abhishek Singharoy, Dongyan Tan

Correspondence

dongyan.tan@stonybrook.edu

In brief

The HP1 protein plays a crucial role in maintaining and spreading heterochromatin. Sokolova et al. employed an integrative structural biology approach to determine the structure of human HP1α in complex with an H2A.Z nucleosome.

Highlights

- The cryo-EM structure of a human HP1α dimer bound to an H2A.Z nucleosome was determined
- H3K9me-independent binding of HP1α is mediated by chromodomain-H2B interactions
- HP1α promotes DNA unwrapping near the nucleosome entry/exit site

Sokolova et al., 2024, Structure *32*, 2094–2106
November 7, 2024
https://doi.org/10.1016/j.str.2024.09.013

CellPress

CellPress
OPEN ACCESS

Structure

Article

Structural mechanism of HP1α-dependent transcriptional repression and chromatin compaction

Vladyslava Sokolova,[1,8] Jacob Miratsky,[2,8] Vladimir Svetlov,[3,4] Michael Brenowitz,[5] John Vant,[2] Tyler S. Lewis,[1] Kelly Dryden,[6] Gahyun Lee,[1] Shayan Sarkar,[7] Evgeny Nudler,[3,4] Abhishek Singharoy,[2] and Dongyan Tan[1,9,*]

[1]Department of Pharmacological Sciences, Stony Brook University, Stony Brook, NY, USA
[2]School of Molecular Sciences, Arizona State University, Tempe, AZ, USA
[3]Department of Biochemistry and Molecular Pharmacology, New York University Grossman School of Medicine, New York, NY, USA
[4]Howard Hughes Medical Institute, Chevy Chase, MD, USA
[5]Departments of Biochemistry and Molecular Pharmacology, Albert Einstein College of Medicine, Bronx, NY, USA
[6]Molecular Physiology and Biological Physics, University of Virginia, Charlottesville, VA 22903, USA
[7]Department of Pathology, Stony Brook University, Stony Brook, NY 11794, USA
[8]These authors contributed equally
[9]Lead contact
*Correspondence: dongyan.tan@stonybrook.edu
https://doi.org/10.1016/j.str.2024.09.013

SUMMARY

Heterochromatin protein 1 (HP1) plays a central role in establishing and maintaining constitutive heterochromatin. However, the mechanisms underlying HP1-nucleosome interactions and their contributions to heterochromatin functions remain elusive. Here, we present the cryoelectron microscopy (cryo-EM) structure of an HP1α dimer bound to an H2A.Z-nucleosome, revealing two distinct HP1α-nucleosome interfaces. The primary HP1α binding site is located at the N terminus of histone H3, specifically at the trimethylated lysine 9 (K9me3) region, while a secondary binding site is situated near histone H2B, close to nucleosome superhelical location 4 (SHL4). Our biochemical data further demonstrates that HP1α binding influences the dynamics of DNA on the nucleosome. It promotes DNA unwrapping near the nucleosome entry and exit sites while concurrently restricting DNA accessibility in the vicinity of SHL4. Our study offers a model for HP1α-mediated heterochromatin maintenance and gene silencing. It also sheds light on the H3K9me-independent role of HP1 in responding to DNA damage.

INTRODUCTION

Constitutive heterochromatin is of fundamental importance to genome stability and the regulation of gene expression. It is characterized by a high copy number of tandem repeats and an enrichment of methylation at lysine 9 of histone H3 (H3K9me). The nuclear protein HP1, which possesses a chromodomain (CD) recognizing and binding to H3K9me, serves as a major component of the constitutive heterochromatin. Recent biophysical studies indicate that HP1 can self-associate to form phase-separated liquid droplets,[1–3] a property believed to be essential for HP1-dependent chromatin compaction. Despite these reports and extensive studies in the past few decades, how HP1 interacts with nucleosomes at the molecular level and how such interactions enable HP1 to fulfill its multifunctional role in the nucleus remain elusive. Multiple studies suggest that the CD-H3K9me interaction alone is insufficient for productive and stable HP1 interactions within the heterochromatin and that other domains are speculated to contribute to HP1 binding to nucleosomes.[4,5] Additional chromatin structural proteins such as histone variant H2A.Z, were also implicated in HP1 recruitment to certain heterochromatin regions in cells.[6] Histone variant H2A.Z is predominantly found at the +1 nucleosomes at the transcription start site (TSS) of active genes, but it is also a consistent feature of pericentric heterochromatin.[7–10] Multiple lines of studies have demonstrated that HP1α directly interacts with H2A.Z-containing nucleosomes *in vivo* and H2A.Z promotes HP1α-mediated chromatin folding.[8,11] Given the existing knowledge, it was proposed that H2A.Z contributes to the maintenance of the stably bound HP1α population in mitotic pericentric heterochromatin.[6]

HP1 is a highly conserved protein with three isoforms in mammals, HP1α, HP1β, and HP1γ. HP1α and HP1β are primarily found in constitutive heterochromatin such as centromere and telomere, while HP1γ is found in both heterochromatin and euchromatin regions.[12–15] All HP1 proteins adopt a tripartite structure (Figure 1A), consisting of two globular domains, the N-terminal CD and the C-terminal chromoshadow domain (CSD). CD and CSD are conserved and homologous to each other. In addition to mediate homodimerization of HP1,[16,17] CSD has been shown to interact with proteins carrying the conserved pentapeptide motif (PxVxL).[18] CD and

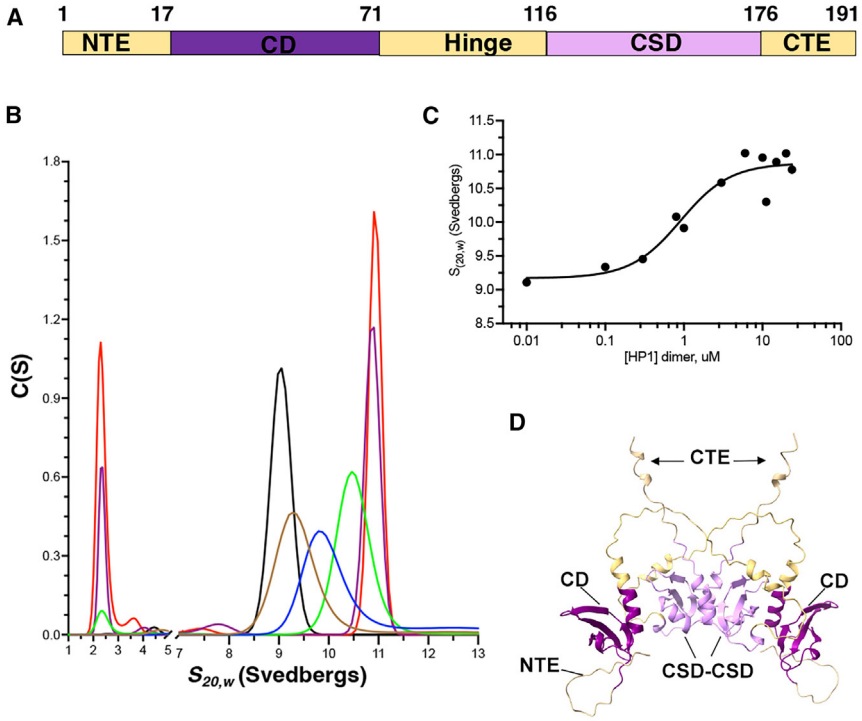

Figure 1. The stoichiometry of the human HP1α-H2A.Z nucleosome complex

(A) Domain architecture of the human HP1α protein.

(B) Representative c(s) distributions determined for the HP1α titration of nucleosome. The nucleosome and nucleosome-HP1α complex peaks span from 9 to 11 $S_{20,w}$. The nucleosome concentration is 0.16 μM HP1α concentrations shown are 0 (black), 0.3 (brown), 0.8 (blue), 3.0 (green), 10.0 (purple), and 20.0 (red) μM. The low $S_{20,w}$ report unbound HP1α at the upper titration plateau.

(C) The HP1α-nucleosome binding isotherm is well fit by the Hill equation with R^2 = 0.9152, K_d = 0.85 (0.52, 1.29) μM, n_H = 1.3 (0.7, 2.5), and lower and upper limits of 9.2 (8.9, 9.4) and 10.9 (10.7, 11.4) *S*, respectively.

(D) Alpha-fold predicted structure of human HP1α dimer.

CSD are connected by the variable and disordered hinge region (HR) (Figure S1A). An early study showed that HR contributes to the localization of HP1 to heterochromatin.[19] Subsequent *in-vitro* studies revealed a more complex picture regarding the binding properties of HR. A cross-linking and mass spectrometry experiment of human HP1β revealed a few cross-linked sites between the HR and histone H3, although various mutations in the HR region do not significantly affect its binding to chromatin.[20] Several studies, nonetheless, confirm the ability of HR to interact with nucleic acids in a sequence-unspecific manner.[19,21,22] In additional to these three domains, the proteins have two short disordered tails at each respective end, the N-terminal extension (NTE) and the C-terminal extension (CTE) (Figures 1A and S1A). The functions of these two domains remain unclear.

The flexible nature of the HP1 protein poses a significant challenge for structural studies of the full-length protein and of HP1 in complex with nucleosomes. Two recent cryo-EM studies revealed low-resolution structures of HP1 in complexes with mono-nucleosomes and with di-nucleosomes.[23,24] Despite these structures, the influence of HP1-nucleosome interactions on the structure and dynamics of chromatin remains enigmatic. To gain insights into the mechanism-of-action of this important epigenetic regulator and its interplays with variant H2A.Z in heterochromatin maintenance, we applied an integrative structural biology approach to dissect the interactions between human HP1α and H2A.Z nucleosome. Using cryoelectron microscopy (cryo-EM) and molecular dynamic flexible fitting (MDFF), we obtained a model of an HP1α dimer bound to an H2A.Z nucleosome. The model reveals that in addition to the primary CD contacting the N terminus of histone H3 and the C terminus of H2A.Z, the second CD interacts with the nucleosome through a new binding site near histone H2B at the superhelical location 4 (SHL4). We have validated this model and confirmed both interacting interfaces with cross-linking mass spectrometry (XL-MS). Our model, supplemented with biochemical data, also revealed that HP1α binding enhances the flexibility of terminal DNAs while simultaneously protects the internal DNA on the nucleosome.

RESULTS

The stoichiometry of the human HP1α-H2A.Z nucleosome complex

Previous research indicated that Swi6 (the *S. pombe* homolog of human HP1α) forms tight dimers and weak higher order oligomers in solution, with two dimers potentially binding to a single nucleosome.[24,25] To determine if the human HP1α protein follows a similar oligomerization pattern, we analyzed the assembly of HP1α by sedimentation velocity analytical ultracentrifugation (SV-AUC). The sedimentation coefficient and the apparent molecular weight of the dominant peak are consistent with HP1α being a stable dimer over the analyzed range of protein concentrations (Figures S1E and S1F). The median value of M_w resolved for the dominant peak of the six distributions is 42,876 Da, within 95% of the value of a HP1α dimer calculated from the protein sequence. The two minor peaks at lower and higher $S_{20,w}$ values are consistent with HP1α monomer and tetramer, respectively.

For substrates, we reconstituted mono-nucleosomes instead of oligo-nucleosomes to reduce the impact of potential heterogeneity in structural studies. These nucleosomes contain 208-bp of 601 Widom sequence, a tri-methyl lysine analog (MLA) at Lys9 of histone H3 to mimic the H3K9me3 modification (referred to as H3K9$_c$me3 thereafter) (Figure S1B). These nucleosomes contain either the canonical H2A or the variant H2A.Z. Consistent with a previous report showing enhanced HP1α binding to nucleosome arrays containing H2A.Z,[11] our electro-mobility shift assays (EMSA) analysis shows that HP1α binds more efficiently to H2A.Z-nucleosomes compared to

canonical nucleosomes (Figures S1C and S1D). Therefore, H2A.Z/H3K9$_c$me3-nucleosomes were used to reconstitute HP1α-nucleosome complex for further structural analysis.

We also performed AUC experiment with free H2A.Z/H3K9$_c$me3-nucleosomes and HP1α-H2A.Z/H3K9$_c$me3-nucleosome complex. The c(s) distribution for the nucleosome is dominated (92%) by a symmetric peak for which values of $S_{(20,w)}$ = 9.1 and M_w = 232,578 Da is resolved. The M_w value is 99% of the value calculated for the assembled DNA and histones of the nucleosome. Only trace amounts of faster and slower peaks are evident in the distribution (Figure 1B). Titration of HP1α into a constant amount of nucleosome resulted in a series peaks of increasing $S_{20,w}$ that plateau at $S_{20,w}$ = 10.9 (Figures 1B and 1C). That single, broad intermediate peaks are observed is consistent with rapid, reversible exchange of HP1α and nucleosome. At the highest concentrations of HP1α, increasing amounts of unbound protein are visualized as a low sedimentation rate peak (Figure 1B, orange, magenta, and green lines). An average M_w = 329,506 Da was calculated for the dominant peak of these three highest HP1α concentrations at the upper plateau is 101% of the value calculated for the nucleosome complexed with two HP1α dimers (325,987 Da). Taken together, the SV-AUC results are consistent with two HP1α dimers bound to one nucleosome with ~1 μM affinity. The precision of the best-fit isotherm is insufficient to distinguish if HP1α binding to the nucleosome is cooperative.

Cryo-EM structure reveals asymmetric binding of HP1α dimer on the nucleosomes

To gain structural insights of the interactions between HP1α and nucleosome, we conducted single-particle cryo-EM study. We employed the Grafix method[26] to stabilize and purify the HP1α-H2A.Z/H3K9$_c$me3-nucleosome complex. To maximize the proportion of complexes in the sample, we only collected fractions that showed clear complex formation on native gels and used them for vitrification. Multiple protein preparations were used for single-particle cryo-EM experiments, resulting in a substantial dataset (Figures S2A and S2C). Although certain 2D class averages reveal blurry densities on both sides of the nucleosome (Figure S2B), most classes in multiple rounds of 3D classification showed HP1 densities on only one side of the nucleosome (Figure S2C), representing one bound HP1α dimer. We suspect that the apparent difference in complex stoichiometry shown in the cryo-EM data and the AUC results likely arises from the limitation of image analysis, where simultaneously aligning and resolving two flexibly bound HP1α dimers on the same nucleosome remains challenging.

Consensus 3D refinement of the best class produced a density map with an average resolution of 6.3 Å (map 1 in Figures S2C and S2G). The HP1α densities in the map range from 6 to 9 Å (Figure S2E). To improve the map, we performed signal subtraction and focused refinement with two overlapping masks: one contains only the nucleosome and the other contains the HP1α density along with a partial nucleosome (mask 2 and mask 3 in Figure S2C). The resolution of the nucleosome map improved to an average resolution of 3.9 Å (map 3 in Figures S2C and S2G). No improvement in the overall resolution was observed for map 2 (Figures S2C and S2G). However, map 2 shows slightly improved map quality compared to map 1.

To further interpret the map, we performed model building using a strategy that combine cascade or cMDFF,[27] and modeling employing limited data (MELD).[28] Specifically, we used domains from the Alphafold structure of human HP1α (also called CBX5) (Figure 1D)[29,30] and the crystal structures of H2A.Z nucleosome to construct an initial model. Although the limited resolution in the HP1α dimer region poses challenges, some secondary structures can be clearly seen in map 2 (Figure S2D). This, along with the fact that HP1α forms a dimer in our experiments and that CSD is known to mediate dimerization of the protein, guided our initial model building. We used three molecules (two CDs and one CSD-CSD dimer, with the NTE, hinge regions, and CTE removed) and performed rigid-body docking to determine their positions and orientation. Notably, while the positions of the CDs and the orientation of one CSD relative to the nucleosome surface can be determined, the exact configuration of the CSD-CSD dimers and the rest of the protein remains ambiguous. The initial model was then used for refinement and optimization in cMDFF and MELD simulation (Figure S3).

The resulting model revealed an asymmetric HP1α dimer packed against the H2A.Z/H3K9$_c$me3 nucleosome (Figures 2A and 2B; Video S1) through two interfaces. The primary interface was mediated by a CD (referred as CD1 in the current study) near the SHL0 position, the histone H3 αN helix, and the H2A.Z C-terminal docking domain (left panel in Figure 2B). The second CD of the HP1α dimer (referred as CD2 in the current study) was situated on the opposite side of the dyad near SHL4 (middle panel in Figure 2B). CD2, along with the H2A.Z N terminus and the H2B C terminus in close proximity, form the second interface.

The CSD-CSD dimer spans a large nucleosome surface, from histone H4 near the dyad to histone H2B, without coming into close contact with the nucleosome (right panel in Figure 2B). The three disordered loops (NTE, HR, and CTE) were largely unresolved in the cryo-EM density map, contributing to the low resolution of the HP1α density in the map. Consequently, they could not be reliably modeled. Both NTEs preceding the CDs are absent from the final model, as rigid-body fitting revealed no assignable density for these regions, reflecting their disordered nature. Similarly, CTE1 was not included in the final model. CTE2 in our model adopts an α helix configuration, as predicted by Alphafold, pointing toward SHL0 (Figure 2B). The exact configurations of the hinge regions cannot be determined in our model.

Upon initial inspection of map 1 and map 3, we also noticed that their DNA ends were notably shorter than usual (Figure 2C). To determine whether this feature is a result of HP1α binding to nucleosomes or the incorporation of variant H2A.Z, we determined a 3.5 Å cryo-EM structure of the free H2A.Z/H3K9$_c$me3 nucleosome prepared under the same condition (Figure S5). A comparison of the nucleosome structures revealed about 107 bps DNA in the HP1α-nucleosome complex, while 130 bps of DNA were resolved in the free H2A.Z/H3K9$_c$me3 nucleosome model (Figure 2C). Additionally, the HP1α-nucleosome complex displayed symmetrical DNA ends, while the free H2A.Z/H3K9$_c$me3 nucleosome contains asymmetric DNA ends (Figure S6). The latter aligns with previous reports showing flexible and asymmetric terminal DNAs in nucleosomes containing histone variant H2A.Z.[31,32] Although we cannot rule out the existence of sequence-dependent dynamic of DNA termini on the

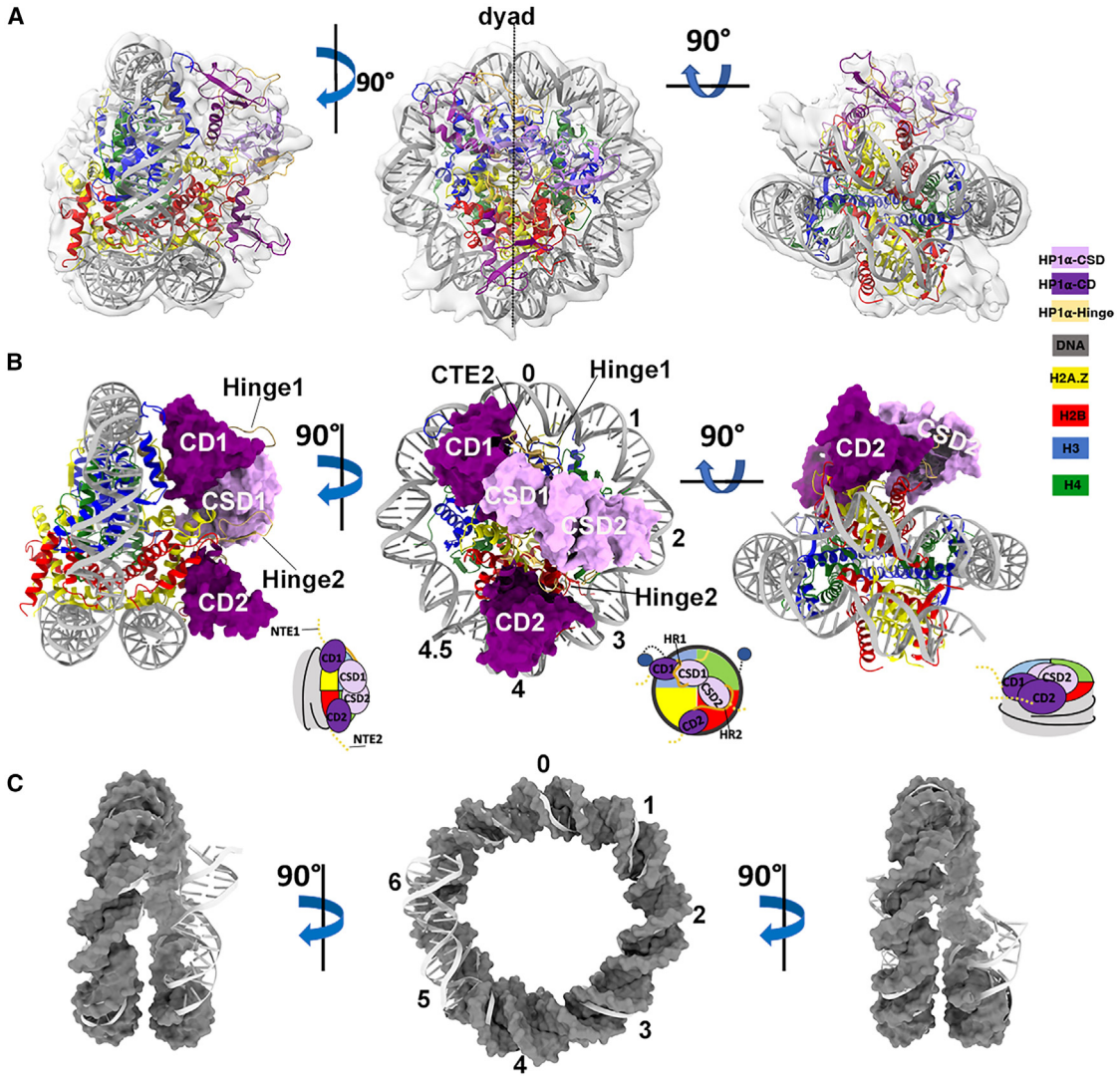

Figure 2. Cryo-EM Structure reveals an asymmetric HP1α dimer on the H2A.Z nucleosome

(A) MDFF model of the HP1α dimer in complex with a K9me3-H2A.Z nucleosome fitted into the consensus refined map (80% transparency),in three different views. HP1α and H2A.Z nucleosome are shown in ribbon diagram.

(B) The MDFF model color coded accordingly in the same three views as in (A). The H2A.Z nucleosome is shown in ribbon diagram and the HP1α dimer in molecular surface mode.

(C) The DNA in the HP1α- K9me3-H2A.Z nucleosome complex (molecular surface mode) is overlaid onto the DNA in the free K9me3-H2A.Z nucleosome (ribbon diagram). Histone cores and HP1α were removed for simplicity.

free H2A.Z/H3K9cme3 nucleosomes, we speculate that the former is the result of the presence of two copies of HP1α dimers on the nucleosome.

CSD mediates HP1α dimerization without direct contact with nucleosomes

Multiple previous atomic models have shown that HP1 CSD, in isolation, form a dimer hinged on their C-terminal α helices with a pseudo 2-fold symmetry[33,34] (Figure S4B). Map 2 shows that the CSD1 region is noisy and poorly resolved, while the CSD2 region shows clearly two helices and a loop (helices αA and αB in Figures 3B and 3C, Videos S2 and S3). The latter allows us to model the CSD-CSD dimer into the density map using rigid body docking. We applied the same CSD-CSD configuration from the crystal structures during initial model building. The final model shows that the αA and αB helices of each CSD monomer form a barrel-like dimer interface (Figures S4C and S4D). Upon further inspection of the final 3D model, we observed possible conformational changes of the dimer compared to the crystal structure of the *Drosophila* HP1 CSD-CSD dimer in complex with an H3 peptide (PDB: 5ti1) (Figure S4D).[34] Specifically, the two CSDs are positioned further apart from each other in our model (Figure S4C). While CSD1 largely adopt the canonical fold of the chromo shadow domain as its *Drosophila* counterpart, structural changes were observed in the β1, β2 strands, and their connecting loop in CSD2 (Figure S4D). We speculate that these

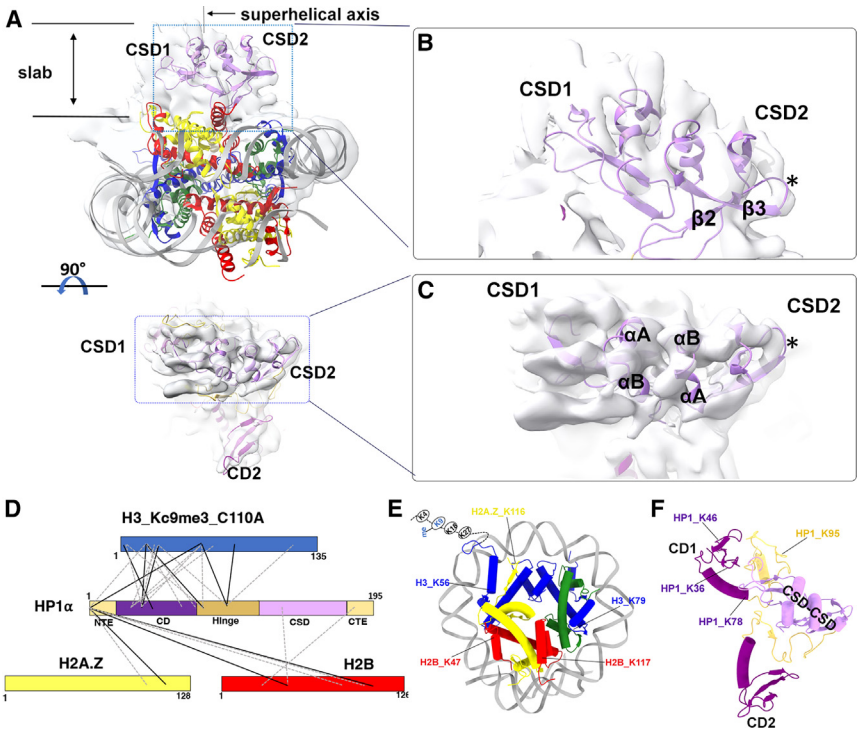

Figure 3. CSD mediates HP1α dimerization without direct contacts with the nucleosome

(A) The MDFF model fitted into the focused refined density map of HP1α-H2A.Z nucleosome (map2 in Figure S3C) in two different views. For simplicity, the two CDs are not shown. For better clarity of the HP1α dimer, only a slab of the volume in the top panel is shown in the bottom panel. The two CSD protomers are indicated and highlighted in blue dotted boxes. The map was low-pass filtered to 6 Å. The superhelical axis is indicated.

(B) Close-up view of the CSD-CSD region highlighted in the top panel in (A). β2 and β3 in the CSD2 domain and the loop (highlighted with an asterisk) connecting the two β strands are labeled.

(C) Close-up view of the CSD-CSD region highlighted in the bottom panel in (A). The four helices made up of the dimer interface are labeled.

(D) Cross-links between HP1α and histones identified by XL-MS. Solid lines are common cross-links identified from two experiments. Dotted lines are unique cross-links identified in only one of the experiments.

(E) Cross-links mapped on the nucleosome from the current model.

(F) Cross-links mapped on the HP1α dimer from the current model.

changes accentuate the asymmetry of the CSD-CSD dimer, explaining the overall asymmetric binding of the HP1α dimer on the nucleosome. It is worth noting that due to the low resolution of the HP1 interaction interface, the placement and conformation of CSD-CSD dimer (especially CSD1) is a proposal that needs further validation through independent method. The structure model, along with the AUC data, suggests that the HP1α dimeric interface in the free form is distinct from that in its nucleosome-bound form.

The CTE, which immediately follows the CSD in HP1, has previously been found to interact with various chromatin factors.[35] Although the precise function and the nature of such interactions remains unknown. As the exact configuration of the CTEs could not be precisely defined in the current structure, we reason that the CTE1 in the model largely remains disordered in the HP1-nucleosome complex. To validate the model and to gain further insights into the HP1-nucleosome interacting interfaces, we conducted XL-MS experiments to probe domain interactions in both free HP1α and HP1α-nucleosome complex. In our analysis of free HP1α, we observed numerous inter-HP1α cross-links, particularly in the hinge, CSD, and CTE regions, suggesting a propensity for self-association of HP1α in these regions (Figure S4A). Overall, our result implies a compact, auto-inhibited state adopted by HP1α in solution, in line with previous findings,[1] The XL-MS experiments also revealed common cross-links between HP1α and the histones (Table S2). The majority of these cross-links involve interactions between HP1α and the H3 N terminus (Figures 3D–3F). Additionally, the N-terminal tail of HP1α cross-linked with both H2B and H2A.Z C terminus, suggesting their spatial proximity. Conversely, only a few unique cross-links, but no common cross-links, were detected between histones and CSD and CTE. It is worth noting that we cannot rule out direct interactions between the CSD-CSD dimer and the histone octamer, due to the limited resolution and noisy densities at the interaction interface. Based on the XL-MS data and taken into consideration of the cryo-EM result, we propose that both CTE and CSD-CSD were further from the nucleosome surface and do not engage in stable and direct interactions with the nucleosome. We further speculate that the CTEs remain mobile and accessible in the HP1α-H2A.Z nucleosome complex. To test this hypothesis, we conducted binding assays using a truncated HP1α (HP1α ΔC) from which the CTE was removed. Through EMSA analysis, we demonstrated that HP1α ΔC binds to H2A.Z nucleosomes with an affinity similar to that of the full-length HP1α (Figure S1D), confirming our hypothesis. In summary, we conclude that the CSD contributes to the protein dimerization and HP1α stability on nucleosomes without directly engaging the substrate. Our data also indicates that while both CSD and CTE can form transient interactions with the nucleosome, they do not significantly contribute to nucleosome binding.

The interaction between CD1-H3-H2A.Z forms the primary interface between the HP1α dimer and the nucleosome

Our model revealed two distinct interfaces of HP1α on the nucleosome, both facilitated by the CD. The primary interface, located near the nucleosome SHL0 position, comprises CD1, histone H3 and, H2A.Z (Figures 4A and 4B). XL-MS data confirmed the existence of this interface, showing cross-links between HP1α CD and H3 N terminus, HP1α NTE and the H2A.Z C-terminal extension, HP1α NTE and H2B (Figure 3D). This interface plays a pivotal role in HP1α recognizing and binding the tri-methylation at lysine 9 of H3, as depicted in our structure. Although the

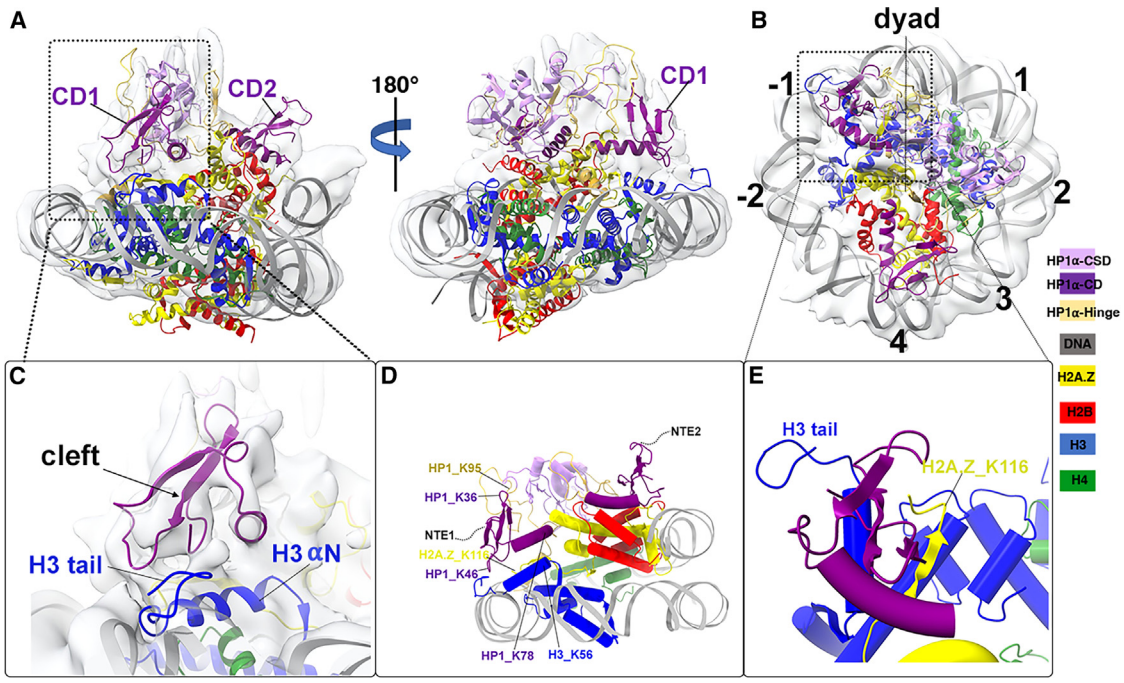

Figure 4. The interaction between CD1-H3-H2A.Z forms the primary interface between the HP1α dimer and the nucleosome

(A) Ribbon diagram of the MDFF model fits into the focused refined map of HP1α dimer with partial H2A.Z nucleosome (map2 in the Figures S3 and S4) in two different views. The density map was low-pass filtered to 6 Å. The primary interacting interface is highlighted in black dotted box.

(B) The model in map 2 looking down from the superhelical axis. The dyad and the SHL positions are labeled.

(C) Close-up view of the primary interface shown in the black box in (A), showing the fit of the CD1 in the density map.

(D) Cross-links at the primary interface identified by XL-MS.

(E) Close-up view of the primary interface shown in the black dotted box in (B), to show the common cross-link between HP1α NTE1 and the H2A.Z C-terminal tail (K116).

CD1-H3K9me3 motif remains unresolved in our cryo-EM map, our model captures the close contact of the CD of a full-length HP1 dimer with histone H3 in the nucleosome. XL-MS experiments unveil cross-links not only in the flexible loop of CD1 but also in its α1 helix along with a lysine situated proximally to the hinge region (Figure 4D). Common cross-links on histone H3 were detected on multiple lysines at the N-terminal tail as well as on the αN helix of H3 (Figure 4D). The close spatial proximity of these cross-linked residues, as depicted in the structural model, aligns excellently with the CD1-nucleosome arrangement in our structural model. In addition to H3, Lysine 116 of H2A.Z on its C-terminal tail is cross-linked with the HP1α NTE1, as demonstrated in the XL-MS results (Figures 3D and 4E). This outcome not only affirms the close contact between the H2A.Z C-terminal tail and the HP1α NTE1 but also suggests that the characteristic residues of H2A.Z at its C terminus contribute to its interactions with HP1α *in vivo*.

Histone H3 αN helix is known to make important contacts with the last turn of DNA at the edge of the nucleosome.[36] Alterations of the H3 N-terminal tail and the adjoining H3 αN helix have been shown to perturb DNA wrapping and histone dimer exchange on nucleosome.[37] Furthermore, this H3-dependent nucleosome dynamics is sensitive to changes in the H2A C-terminal extension, which contacts H3 αN helix to influences terminal DNA dynamics.[31,38] Our current model demonstrated that these structural motifs constitute the primary binding site for HP1α dimer. We propose that CD1 binding to this site interfere with the histone-DNA interactions mediated by H3 N terminus and H2A.Z C terminus, thereby increasing DNA flexibility at the edge of the nucleosome.

Additionally, we compared the CD1 in the current model to the crystal structure of its *Drosophila* counterpart (PDB: 1KNE).[39] The comparison revealed that both structures exhibit the canonical fold of the conserved chromo domain (Figure S4E). The *Drosophila* HP1 CD and its mouse counterpart for HP1β both employ an induce-fit cleft to interact with the H3 peptide in a β sandwich conformation[39,40] (Figure S4E). The cleft is in close proximity to the H3 tail and H3 αN helix in the current model (Figure 4C), suggesting that HP1α CD1 employs the same mechanism as other HP1 homologs in recognizing the H3K9me modification on nucleosome.

CD2-H2B form the second interacting interface between HP1α and the nucleosome

The secondary HP1α-nucleosome interface, composed of CD2 and histone H2B (Figures 5A and 5B), is located at a distance from the primary binding site, situated on the opposite end of the dyad and near SHL4 in our model (Figures 2A and 2B). In our model, the α helix of CD2 interacts with α1 helix of H2B, while the loop in CD2 contacts the H2B αC helix (Figure 5B). Similar to the CD1-H3 interface, the NTE2 preceding CD2 is absent in the model. According to our model, NTE2 would be outward-facing

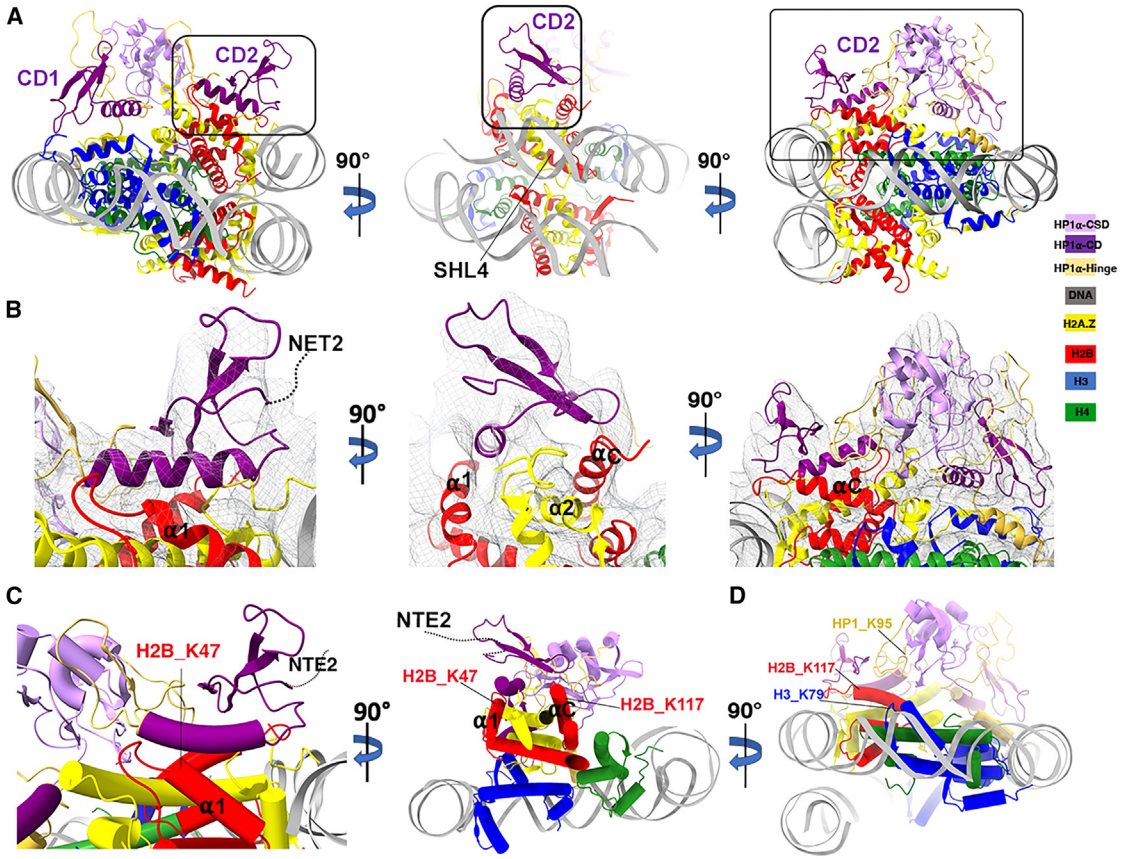

Figure 5. CD2-H2B form the second interacting interface between HP1α and the nucleosome

(A) The MDFF model in three different views. The second interface mediated by CD2 and H2B is highlighted with black box.

(B) Close-up views of the second interface as shown in (A) in its respective angle. The MDFF model was fitted into map2 (low-pass filtered to 6 Å) to show the overall fit of CD2 in the density map.

(C) The cross-linked H2B lysine identified by XL-MS are mapped and labeled in the model (rod diagram). The views correspond to the left and middle panels in (B). The two lysine are in H2B α1 helix and αC helix respectively. The putative position of HP1α NTE2 (not resolved in the model) is indicated as a dotted curve.

(D) A cross-link between H3 K79 and a lysine at the HP1α hinge region (K95) is mapped in the model. The view corresponds to the right panel in (B).

(indicated as a dotted line in Figure 5C), suggesting that it remains mobile within the complex. In our comparative analysis, we found that the CD2 in our model closely resembles the crystal structure of *Drosophila* CD (Figure S4E). We therefore conclude that both CDs in the HP1α dimer adopt a conserved and nearly identical fold as its *Drosophila* counterpart.

Our XL-MS results reveal two common cross-links and several unique cross-links between H2B and the NTE2 of HP1α (Figure 3D), providing direct evidence for the existence of this interacting interface. When mapped on the model, these common cross-links appear on H2B α1 helix (K47 in Figure 5C) and the αC helix of H2B (K117 in Figures 5C and 5D). This XL-MS result further validates our model. Therefore, we conclude that the CD2-H2B interactions in our model represent a previously unreported binding interface between HP1α and the nucleosome. This binding site, composed of the H2B α1 and αC helices, is distinct from the primary binding site on H3 tail and H2A C terminus, and it is independent of H3K9 methylations.

It is worth noting that in the current structure, the 601 Widom DNA was found to be mobile at both terminus and thus was resolved only up to SHL4.5/-4.5 location (Figure 2C). DNA segments near SHL4 and SHL5 are known to interact with the C terminus of H2B and N terminus of H2A in the major-type nucleosome.[36] It is thus tempting to speculate that CD2 binding to these histone motifs may stabilize the histone-DNA interaction and thus protects DNA near SHL4 to SHL5.

The effects of HP1α-binding on nucleosome DNA accessibility

Terminal DNA breathing is an inherent property of nucleosome dynamics. Increased terminal DNA unwrapping has been observed for nucleosomes containing histone variants H2A.Z and H2A.B.[31,32,41] In certain structures, nucleosome complexes with chromatin remodelers and RNA polymerases have shown DNA-end deformation or peeling.[42] To the best of our knowledge, there have been no reports of enhanced DNA breathing associated with epigenetic repressors and heterochromatin proteins. To delve deeper into HP1α's potential to influence terminal DNA flexibility, as suggested by our cryo-EM model, we conducted the DNA accessibility assay using a micrococcal nuclease (MNase). MNase cleaves DNA in a

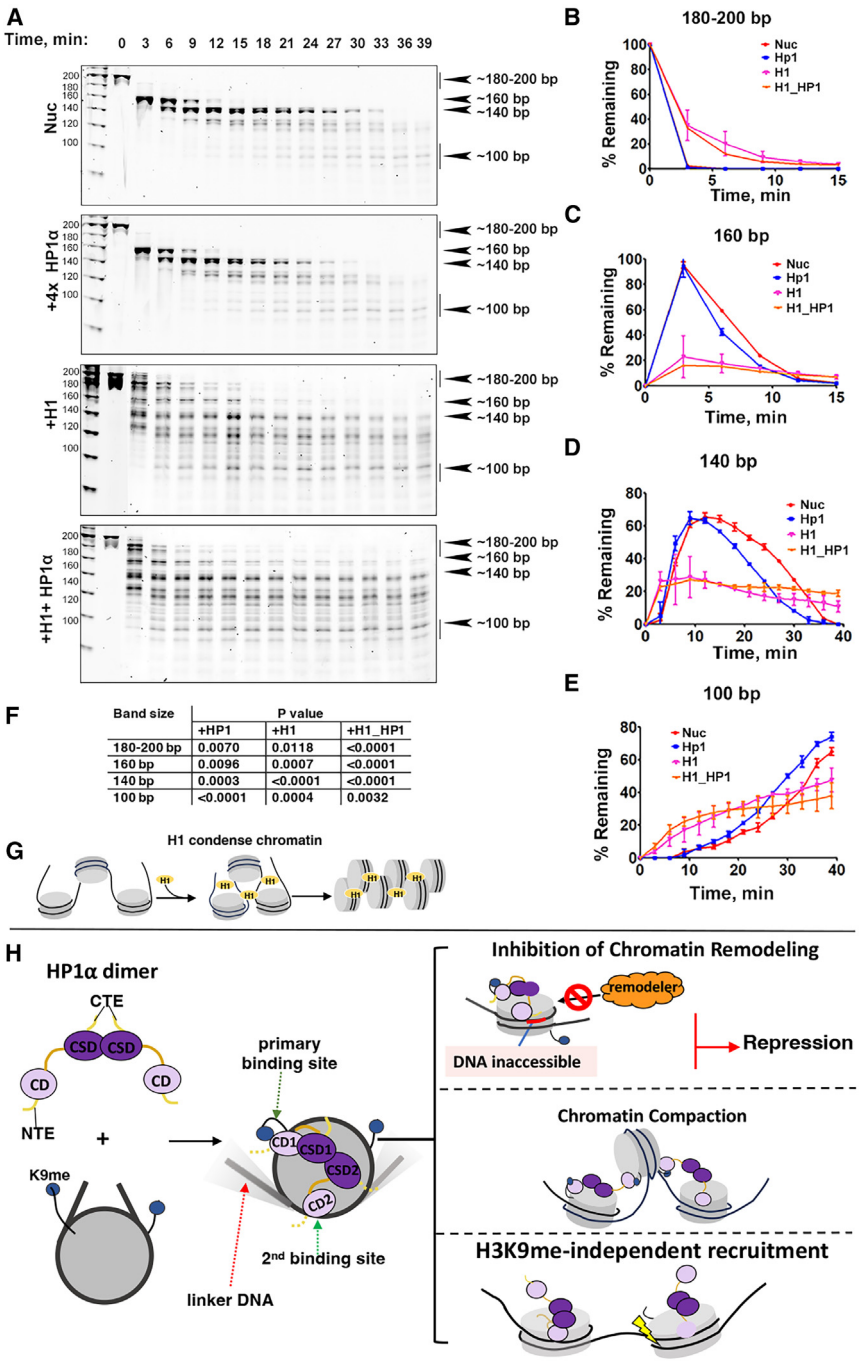

Band size	P value		
	+HP1	+H1	+H1_HP1
180-200 bp	0.0070	0.0118	<0.0001
160 bp	0.0096	0.0007	<0.0001
140 bp	0.0003	<0.0001	<0.0001
100 bp	<0.0001	0.0004	0.0032

Figure 6. The effects of HP1α-binding on nucleosome DNA accessibility

(A) Representative acrylamide gels of the MNase assay with no HP1α, 4x excess of HP1α, 1x H1, and 1x H1+ 4x HP1α, respectively. The digestion products of different sizes (180–200, 160, 140, and 100-bp) are labeled.

(B) Quantification of the 180–200 bp DNA products shown in (A), representing the fraction of digested nucleosome DNA as a function of time. Data are mean ± SD, $n = 3$.

(C) Quantification of the 160 bp DNA products shown in (A). Data are mean ± SD, $n = 3$.

(D) Quantification of the 140–145 bp DNA product shown in (A). Data are mean ± SD, $n = 3$.

(E) Quantification of the 100 bp DNA products shown in (A). Data are mean ± SD, $n = 3$.

(F) p values of the experiments shown in (B), (C), (D), and (E).

(G) Schematic of the model for H1-mediated chromatin compaction.

(H) Schematic of the proposed model of HP1α-mediated gene repression, heterochromatin maintenance, and H3K9me-independent role in DNA damaged response.

sequence-unspecific manner, allowing us to access changes in nucleosomal DNA accessibility resulting from HP1α binding. Our MNase digestion of the K9me3-H2A.Z nucleosome generated a ladder-like pattern that evolved over time and eventually dissolved completely after 40 min (Figure 6A). As expected, the presence of stoichiometric histone H1, known for its role in stabilizing higher-order chromatin structures through interactions with linker DNAs (Figure 6G), protected linker DNA and slowed down MNase digestion of K9me3-H2A.Z nucleosomes.[43–45] This protection is evident from the appearance of two higher molecular weight bands at 200 bp and 160 bp (see Figures 6A–6C), which were entirely absent in reactions with free K9me3-H2A.Z nucleosomes.

We then explored how HP1α influences MNase digestion of K9me3-H2A.Z nucleosomes. When a 4-fold excess of HP1α (equivalent to two HP1α dimers) was introduced, we observed accelerated digestion over time, particularly for two DNA bands ranging in size from 140 to 147-bp (see Figures 6A and 6D). This observation aligns with our cryo-EM model's prediction that HP1α binding enhances the mobility and accessibility of terminal DNAs. Intriguingly, at later time points, we noticed a reverse trend. In the HP1α-H2A.Z nucleosome reaction, DNA bands approximately 100 bp in size persisted while they continued to degrade in the control reaction (see Figures 6A and 6E). A 100 bp product corresponds to the digestion of the 601 Widom sequence at or near SHL-4.5, which is the CD2 binding site revealed by our cryo-EM model. The differences between samples were reproducible and statistically significant (Figure 6F). Therefore, our MNase results collectively suggest that HP1α enhances terminal DNA unwrapping while also stabilizing and protecting internal DNA.

DISCUSSION

Implications for HP1α-mediated transcription repression

In this study, we employed a strategy that combines cryo-EM, MDFF, and XL-MS to obtain a structural model of human HP1α

dimer bound to an H2A.Z nucleosome. Our model illustrates how the HP1α dimer asymmetrically engages nucleosomes through extensive interactions between the two CDs and the nucleosome surface. An intriguing discovery from our study is the identification of a second binding site for HP1α on histone H2B, which is independent of H3K9 methylations. Our model also reveals that the function of the HP1α CSD is primarily to mediate HP1 dimerization, without directly engaging in interactions with the nucleosome. Our biochemical data demonstrates that these two CD bindings have contrasting effects on nucleosome DNA accessibility. These findings carry significant implications for our understanding of the multifaceted role of HP1α in shaping heterochromatin and mediating gene expression.

We propose that HP1 binding modulates the structure-dynamics of the nucleosome, resulting in enhanced terminal DNA flexibility while simultaneously protecting internal DNA. Given that many ATP-dependent chromatin remodelers rely on the structural features such as the acidic patch to interact with nucleosomes,[46] it is conceivable that HP1 binding inevitably compete with chromatin remodelers' actions on chromatin. Additionally, the binding of HP1 CD domain to histone H2B near SHL4 may further impeded remodelers on nucleosome and their processive DNA translocation activity (Figure 6H).

Implications for HP1α-mediated chromatin compaction and maintenance

Linker histone H1, a vital chromatin protein in higher organisms, is renowned for its role in promoting the assembly of higher-order chromatin structures and stabilizing chromatin fibers. Through binding to linker DNAs, H1 forms a stem-like structure with reduced entry-exit angles termed a chromatosome, thereby contributing to the formation of chromatin fibers.[47] Our data suggest that HP1α employs a mechanism distinct from that of H1 to facilitate chromatin folding. Instead of constraining entry-exit DNA angles, HP1α increases the flexibility of terminal DNA on nucleosomes, an unexpected outcome resulting from interactions at the primary binding site on histones H3 and H2A. Consequently, in contrast to the regular helical structure observed in *in-vitro* reconstituted H1-chromatin fibers,[48] we propose that in HP1α-chromatin region, chromatin fibers adopt a compact yet irregular structure (Figure 6H). In the context of chromatin higher-order structures, we propose that neighboring nucleosomes are brought into proximity by HP1α dimers through interactions involving the chromodomains and the two nucleosome binding sites described above. One possibility is that an HP1α dimer bridges two nucleosomes only through the CD-H3K9me interactions. Or an HP1α dimer can bridge two nucleosomes through both the CD-H3K9me interaction and the CD-H2B interaction (Figure 6H). This model aligns with the idea that the modular nature of HP1α allows the formation of different types of HP1-nucleosome complexes, which facilitate chromatin compaction.[8,49] Whether the two other HP1 isoforms use a similar mechanism to interact and regulate chromatin remains to be tested.

It is worth noting that a previous low-resolution HP1-dinucleosome cryo-EM structure shows a slightly different model of interaction: a symmetrical HP1 dimer bridging two nucleosomes while the linker DNA makes no contact with the HP1.[23] Similarly, we did not observe direct DNA interactions with the hinge region of HP1α in our structure. However, our model indicates the existence of a new HP1-biding site on H2B, which breaks the symmetry in the absence of an adjacent H3K9me3-containing nucleosome.

We further propose that the flexible linker DNA enables a higher degree of twisting of linker DNAs between two adjacent nucleosomes, facilitating the formation of compact yet irregular heterochromatin. Although flexible linker DNA may lead to potential higher entropy, HP1-mediated chromatin compaction can also restrict overall nucleosome mobility in the heterochromatin region, compensating for the increase in entropy. Importantly, our model suggests that HP1-heterochromatin is likely polymorphic in nature, aligning closely with recent studies demonstrating that human mitotic chromosomes consist predominantly of irregularly folded chromatin fibers.[50–52]

Chromatin-binding independent of H3K9 methylation

HP1 family proteins are versatile epigenetic regulators with functions outside of heterochromatin maintenance and transcription repression. Early studies indicated a role of HP1 in DNA damage response (DDR).[53,54] While many aspects of this enigmatic but crucial role of HP1 in DDR remain unknown, *in-vivo* studies showed that all three HP1 isoforms are efficiently recruited to DNA damage sites in human cells.[55] This response to DNA damage requires the CSD of HP1, but is independent of H3K9 trimethylation.[55] The structure presented in our study unveils a second nucleosome-binding site on the nucleosome surface near the N terminus of histone H2B and the C terminus of H2A, away from both copies of the methylated H3 tails. Our model supports a previous study indicating that H2A.Z can functional replace H3K9me3 to recruit HP1 in pericentric heterochromatin.[7] Since H2A.Z Lysine 116 at this region can be acetylated or ubiquitinated,[56] our model also suggests that these post-translational modifications (PTMs) may regulate HP1 binding to H2A.Z nucleosomes. Therefore, our structure provides a rational explanation for how HP1 can be recruited to DNA damage sites in an H3K9me-independent manner.

The implication for the role of HP1 CSD

CSD-mediated homodimerization has been extensively studied and well characterized. The CSD-CSD dimer, along with the CTE, creates a hydrophobic-binding site and is believed to facilitate HP1's interaction with many non-histone chromosomal proteins containing PXVXL or related motifs (where X denotes any amino acids).[57,58] In our model, the CSD-CSD hydrophobic binding site is oriented toward the nucleosome surface but does not directly interact with any histones. Additionally, given that H3 is the sole histone containing a PXVXL sequence at its αN helix, it is unlikely that the CSD-CSD hydrophobic pocket makes direct contact with H3 αN helix. Our model also suggests that when both CDs are engaged with the same nucleosome, the HP1α dimer may not be capable of binding to PXVXL-containing proteins through CSD-CSD region. However, since our model supports the idea that the modular structure of HP1 allows it to establish various interactions within itself and to form different types of HP1-nucleosome interactions,[49] it is reasonable to assume that the CSD-CSD hydrophobic-binding site will remain accessible for binding partners where only one CD in the HP1 dimer contacts with nucleosome. Future studies will be necessary to test these hypotheses and to gain further insights into these interactions.

Limitations of the study

Although our work provides a more detailed model for how HP1α interacts with nucleosomes, additional biochemical and structural work is needed to dissect the detailed interacting interface between HP1 and nucleosome and to understand exactly how HP1α facilitates heterochromatin formation a. In particular, the proposed conformation of the CSD-CSD dimerization domain and its placement relative to the nucleosome in our model is based on the low-resolution cryo-EM map and the CS-MS data. This conformation and placement need to be more directly tested with further mutagenesis and improved cryo-EM structural analysis of similar complex or HP1 in complex with oligo-nucleosomes. In addition, the conformation of the HRs cannot be determined in the current study due to the intrinsic disorder nature of this region and the limited resolution of the cryo-EM map.

RESOURCE AVAILABILITY

Lead contact

Further information and requests for resources and reagents should be directed to and will be fulfilled by the lead contact, Dongyan Tan (Dongyan.tan@stonybrook.edu).

Materials availability

This study did not generate new unique reagents. Plasmids generated in this study will be made available on request, but we may require a payment and/or a completed Materials Transfer Agreement if there is potential for commercial application.

Data and code availability

- Structural data have been deposited in the Electron Microscopy Database (https://www.ebi.ac.uk/pdbe/emdb) and the Protein DataBank (https://www.rcsb.org/). EM maps are deposited at the Electron Microscopy Database under accession code EMD-42774 for the HP1α-H2A.Z nucleosome complex (map1), EMD-42690 for focused refined HP1α in complex with partial H2A.Z nucleosome (map2), EMD-42692 for focused refined K9me3_H2A.Z nucleosome (map3), and EMD-42773 for the free K9me3_H2A.Z nucleosome. The protein coordinate of the HP1α-H2A.Z nucleosome complex presented in the paper is deposited at (PDB: 8UXQ). They are publicly available as of the date of publication.
- This paper does not report original code.
- Any additional information required to reanalyze the data reported in this paper is available from the lead contact upon request.

ACKNOWLEDGMENTS

We thank the staff in the Laboratory for BioMolecular Structure (LBMS) for help in data collection. LBMS is supported by the DOE Office of Biological and Environmental Research (KP1607011). This work was also supported by: NIH grant 1R35GM133611 to D.T. NSF grant 1942049 to D.T. Access to the additional instrumentation was supported by the following grants: NIH grant U24 GM116790 to M.Y. and D.T., NIH grant 1S10OD012272-01A1 to H.L. Transmission electron micrographs were recorded at the University of Virginia Molecular Electron Microscopy Core facility (RRID:SCR_019031), which is supported in part by the School of Medicine and built with NIH grant G20-RR31199. In addition, the Titan Krios (S10-RR025067) and K3/GIF (U24-GM116790) were purchased in part or in full with the designated NIH grants.

AUTHOR CONTRIBUTIONS

V. Sokolova, T.S.L., and G.L. prepared the samples for EM study; K.D. collected the cryo-EM data; V. Sokolova performed the biochemical experiment and analysis; D.T. performed cryo-EM image analysis; M.B. performed the AUC experiments and data analysis; J.K. and J.V. performed model building under the supervision of A.S.; V. Svetlov performed the XL-MS experiments under the supervision of E.N.; D.T. oversaw the project and wrote the manuscript with help from all authors.

DECLARATION OF INTERESTS

The authors declare no competing interests.

STAR★METHODS

Detailed methods are provided in the online version of this paper and include the following:

- KEY RESOURCES TABLE
- EXPERIMENTAL MODEL AND STUDY PARTICIPANT DETAILS
- METHOD DETAILS
  - Expression and purification of HP1α
  - Nucleosome reconstitutions
  - SV-AUC
  - MNase assays
  - Nucleosome binding assay
  - Assembly of the HP1α-H2A.Z-H3K9$_c$me3 nucleosome complex for cryo-EM study
  - Cryo-EM sample vitrification
  - Cryo-EM data collection
  - Image analysis
  - Model building and refinement
  - XL-MS and data analysis
- QUANTIFICATION AND STATISTICAL ANALYSIS

SUPPLEMENTAL INFORMATION

Supplemental information can be found online at https://doi.org/10.1016/j.str.2024.09.013.

Received: January 18, 2024
Revised: August 12, 2024
Accepted: September 12, 2024
Published: October 8, 2024

REFERENCES

1. Larson, A.G., Elnatan, D., Keenen, M.M., Trnka, M.J., Johnston, J.B., Burlingame, A.L., Agard, D.A., Redding, S., and Narlikar, G.J. (2017). Liquid droplet formation by HP1alpha suggests a role for phase separation in heterochromatin. Nature *547*, 236–240. https://doi.org/10.1038/nature22822.
2. Sanulli, S., Trnka, M.J., Dharmarajan, V., Tibble, R.W., Pascal, B.D., Burlingame, A.L., Griffin, P.R., Gross, J.D., and Narlikar, G.J. (2019). HP1 reshapes nucleosome core to promote phase separation of heterochromatin. Nature *575*, 390–394. https://doi.org/10.1038/s41586-019-1669-2.
3. Strom, A.R., Emelyanov, A.V., Mir, M., Fyodorov, D.V., Darzacq, X., and Karpen, G.H. (2017). Phase separation drives heterochromatin domain formation. Nature *547*, 241–245. https://doi.org/10.1038/nature22989.
4. Mishima, Y., Watanabe, M., Kawakami, T., Jayasinghe, C.D., Otani, J., Kikugawa, Y., Shirakawa, M., Kimura, H., Nishimura, O., Aimoto, S., et al. (2013). Hinge and chromoshadow of HP1alpha participate in recognition of K9 methylated histone H3 in nucleosomes. J. Mol. Biol. *425*, 54–70. https://doi.org/10.1016/j.jmb.2012.10.018.
5. Zhao, T., Heyduk, T., Allis, C.D., and Eissenberg, J.C. (2000). Heterochromatin protein 1 binds to nucleosomes and DNA *in vitro*. J. Biol. Chem. *275*, 28332–28338. https://doi.org/10.1074/jbc.M003493200.
6. Rangasamy, D., Greaves, I., and Tremethick, D.J. (2004). RNA interference demonstrates a novel role for H2A.Z in chromosome segregation. Nat. Struct. Mol. Biol. *11*, 650–655. https://doi.org/10.1038/nsmb786.

7. Boyarchuk, E., Filipescu, D., Vassias, I., Cantaloube, S., and Almouzni, G. (2014). The histone variant composition of centromeres is controlled by the pericentric heterochromatin state during the cell cycle. J. Cell Sci. *127*, 3347–3359. https://doi.org/10.1242/jcs.148189.

8. Fan, J.Y., Rangasamy, D., Luger, K., and Tremethick, D.J. (2004). H2A.Z alters the nucleosome surface to promote HP1alpha-mediated chromatin fiber folding. Mol. Cell *16*, 655–661. https://doi.org/10.1016/j.molcel.2004.10.023.

9. Greaves, I.K., Rangasamy, D., Ridgway, P., and Tremethick, D.J. (2007). H2A.Z contributes to the unique 3D structure of the centromere. Proc. Natl. Acad. Sci. USA *104*, 525–530. https://doi.org/10.1073/pnas.0607870104.

10. Nekrasov, M., Amrichova, J., Parker, B.J., Soboleva, T.A., Jack, C., Williams, R., Huttley, G.A., and Tremethick, D.J. (2012). Histone H2A.Z inheritance during the cell cycle and its impact on promoter organization and dynamics. Nat. Struct. Mol. Biol. *19*, 1076–1083. https://doi.org/10.1038/nsmb.2424.

11. Ryan, D.P., and Tremethick, D.J. (2018). The interplay between H2A.Z and H3K9 methylation in regulating HP1alpha binding to linker histone-containing chromatin. Nucleic Acids Res. *46*, 9353–9366. https://doi.org/10.1093/nar/gky632.

12. Hayakawa, T., Haraguchi, T., Masumoto, H., and Hiraoka, Y. (2003). Cell cycle behavior of human HP1 subtypes: distinct molecular domains of HP1 are required for their centromeric localization during interphase and metaphase. J. Cell Sci. *116*, 3327–3338. https://doi.org/10.1242/jcs.00635.

13. Smallwood, A., Hon, G.C., Jin, F., Henry, R.E., Espinosa, J.M., and Ren, B. (2012). CBX3 regulates efficient RNA processing genome-wide. Genome Res. *22*, 1426–1436. https://doi.org/10.1101/gr.124818.111.

14. Vakoc, C.R., Mandat, S.A., Olenchock, B.A., and Blobel, G.A. (2005). Histone H3 lysine 9 methylation and HP1gamma are associated with transcription elongation through mammalian chromatin. Mol. Cell *19*, 381–391. https://doi.org/10.1016/j.molcel.2005.06.011.

15. Maison, C., and Almouzni, G. (2004). HP1 and the dynamics of heterochromatin maintenance. Nat. Rev. Mol. Cell Biol. *5*, 296–304. https://doi.org/10.1038/nrm1355.

16. Brasher, S.V., Smith, B.O., Fogh, R.H., Nietlispach, D., Thiru, A., Nielsen, P.R., Broadhurst, R.W., Ball, L.J., Murzina, N.V., and Laue, E.D. (2000). The structure of mouse HP1 suggests a unique mode of single peptide recognition by the shadow chromo domain dimer. EMBO J. *19*, 1587–1597. https://doi.org/10.1093/emboj/19.7.1587.

17. Jacobs, S.A., Taverna, S.D., Zhang, Y., Briggs, S.D., Li, J., Eissenberg, J.C., Allis, C.D., and Khorasanizadeh, S. (2001). Specificity of the HP1 chromo domain for the methylated N-terminus of histone H3. EMBO J. *20*, 5232–5241. https://doi.org/10.1093/emboj/20.18.5232.

18. Meyer-Nava, S., Nieto-Caballero, V.E., Zurita, M., and Valadez-Graham, V. (2020). Insights into HP1a-Chromatin Interactions. Cells *9*, 1866. https://doi.org/10.3390/cells9081866.

19. Meehan, R.R., Kao, C.F., and Pennings, S. (2003). HP1 binding to native chromatin *in vitro* is determined by the hinge region and not by the chromodomain. EMBO J. *22*, 3164–3174. https://doi.org/10.1093/emboj/cdg306.

20. Hiragami-Hamada, K., Soeroes, S., Nikolov, M., Wilkins, B., Kreuz, S., Chen, C., De La Rosa-Velázquez, I.A., Zenn, H.M., Kost, N., Pohl, W., et al. (2016). Dynamic and flexible H3K9me3 bridging via HP1beta dimerization establishes a plastic state of condensed chromatin. Nat. Commun. *7*, 11310. https://doi.org/10.1038/ncomms11310.

21. Maison, C., Bailly, D., Peters, A.H.F.M., Quivy, J.P., Roche, D., Taddei, A., Lachner, M., Jenuwein, T., and Almouzni, G. (2002). Higher-order structure in pericentric heterochromatin involves a distinct pattern of histone modification and an RNA component. Nat. Genet. *30*, 329–334. https://doi.org/10.1038/ng843.

22. Muchardt, C., Guilleme, M., Seeler, J.S., Trouche, D., Dejean, A., and Yaniv, M. (2002). Coordinated methyl and RNA binding is required for heterochromatin localization of mammalian HP1alpha. EMBO Rep. *3*, 975–981. https://doi.org/10.1093/embo-reports/kvf194.

23. Machida, S., Takizawa, Y., Ishimaru, M., Sugita, Y., Sekine, S., Nakayama, J.I., Wolf, M., and Kurumizaka, H. (2018). Structural Basis of Heterochromatin Formation by Human HP1. Mol. Cell *69*, 385–397.e8. https://doi.org/10.1016/j.molcel.2017.12.011.

24. Canzio, D., Liao, M., Naber, N., Pate, E., Larson, A., Wu, S., Marina, D.B., Garcia, J.F., Madhani, H.D., Cooke, R., et al. (2013). A conformational switch in HP1 releases auto-inhibition to drive heterochromatin assembly. Nature *496*, 377–381. https://doi.org/10.1038/nature12032.

25. Canzio, D., Chang, E.Y., Shankar, S., Kuchenbecker, K.M., Simon, M.D., Madhani, H.D., Narlikar, G.J., and Al-Sady, B. (2011). Chromodomain-mediated oligomerization of HP1 suggests a nucleosome-bridging mechanism for heterochromatin assembly. Mol. Cell *41*, 67–81. https://doi.org/10.1016/j.molcel.2010.12.016.

26. Stark, H. (2010). GraFix: stabilization of fragile macromolecular complexes for single particle cryo-EM. Methods Enzymol. *481*, 109–126. https://doi.org/10.1016/S0076-6879(10)81005-5.

27. Singharoy, A., Teo, I., McGreevy, R., Stone, J.E., Zhao, J., and Schulten, K. (2016). Molecular dynamics-based refinement and validation for sub-5 A cryo-electron microscopy maps. Elife *5*, e16105. https://doi.org/10.7554/eLife.16105.

28. MacCallum, J.L., Perez, A., and Dill, K.A. (2015). Determining protein structures by combining semireliable data with atomistic physical models by Bayesian inference. Proc. Natl. Acad. Sci. USA *112*, 6985–6990. https://doi.org/10.1073/pnas.1506788112.

29. Jumper, J., Evans, R., Pritzel, A., Green, T., Figurnov, M., Ronneberger, O., Tunyasuvunakool, K., Bates, R., Žídek, A., Potapenko, A., et al. (2021). Highly accurate protein structure prediction with AlphaFold. Nature *596*, 583–589. https://doi.org/10.1038/s41586-021-03819-2.

30. Varadi, M., Anyango, S., Deshpande, M., Nair, S., Natassia, C., Yordanova, G., Yuan, D., Stroe, O., Wood, G., Laydon, A., et al. (2022). AlphaFold Protein Structure Database: massively expanding the structural coverage of protein-sequence space with high-accuracy models. Nucleic Acids Res. *50*, D439–D444. https://doi.org/10.1093/nar/gkab1061.

31. Lewis, T.S., Sokolova, V., Jung, H., Ng, H., and Tan, D. (2021). Structural basis of chromatin regulation by histone variant H2A. Nucleic Acids Res. *49*, 11379–11391. https://doi.org/10.1093/nar/gkab907.

32. Zhou, M., Dai, L., Li, C., Shi, L., Huang, Y., Guo, Z., Wu, F., Zhu, P., and Zhou, Z. (2021). Structural basis of nucleosome dynamics modulation by histone variants H2A.B and H2A.Z.2.2. EMBO J. *40*, e105907. https://doi.org/10.15252/embj.2020105907.

33. Kang, J., Chaudhary, J., Dong, H., Kim, S., Brautigam, C.A., and Yu, H. (2011). Mitotic centromeric targeting of HP1 and its binding to Sgo1 are dispensable for sister-chromatid cohesion in human cells. Mol. Biol. Cell *22*, 1181–1190. https://doi.org/10.1091/mbc.E11-01-0009.

34. Liu, Y., Qin, S., Lei, M., Tempel, W., Zhang, Y., Loppnau, P., Li, Y., and Min, J. (2017). Peptide recognition by heterochromatin protein 1 (HP1) chromoshadow domains revisited: Plasticity in the pseudosymmetric histone binding site of human HP1. J. Biol. Chem. *292*, 5655–5664. https://doi.org/10.1074/jbc.M116.768374.

35. Huang, Y., Myers, M.P., and Xu, R.M. (2006). Crystal structure of the HP1-EMSY complex reveals an unusual mode of HP1 binding. Structure *14*, 703–712. https://doi.org/10.1016/j.str.2006.01.007.

36. Luger, K., Mäder, A.W., Richmond, R.K., Sargent, D.F., and Richmond, T.J. (1997). Crystal structure of the nucleosome core particle at 2.8 A resolution. Nature *389*, 251–260. https://doi.org/10.1038/38444.

37. Ferreira, H., Somers, J., Webster, R., Flaus, A., and Owen-Hughes, T. (2007). Histone tails and the H3 alphaN helix regulate nucleosome mobility and stability. Mol. Cell Biol. *27*, 4037–4048. https://doi.org/10.1128/MCB.02229-06.

38. Flaus, A., Rencurel, C., Ferreira, H., Wiechens, N., and Owen-Hughes, T. (2004). Sin mutations alter inherent nucleosome mobility. EMBO J. *23*, 343–353. https://doi.org/10.1038/sj.emboj.7600047.

39. Jacobs, S.A., and Khorasanizadeh, S. (2002). Structure of HP1 chromodomain bound to a lysine 9-methylated histone H3 tail. Science *295*, 2080–2083. https://doi.org/10.1126/science.1069473.

40. Nielsen, P.R., Nietlispach, D., Mott, H.R., Callaghan, J., Bannister, A., Kouzarides, T., Murzin, A.G., Murzina, N.V., and Laue, E.D. (2002). Structure of the HP1 chromodomain bound to histone H3 methylated at lysine 9. Nature *416*, 103–107. https://doi.org/10.1038/nature722.

41. Sokolova, V., Sarkar, S., and Tan, D. (2023). Histone variants and chromatin structure, update of advances. Comput. Struct. Biotechnol. J. *21*, 299–311. https://doi.org/10.1016/j.csbj.2022.12.002.

42. Kobayashi, W., and Kurumizaka, H. (2019). Structural transition of the nucleosome during chromatin remodeling and transcription. Curr. Opin. Struct. Biol. *59*, 107–114. https://doi.org/10.1016/j.sbi.2019.07.011.

43. Kornberg, R.D. (1974). Chromatin structure: a repeating unit of histones and DNA. Science *184*, 868–871. https://doi.org/10.1126/science.184.4139.868.

44. Kornberg, R.D., and Thomas, J.O. (1974). Chromatin structure; oligomers of the histones. Science *184*, 865–868. https://doi.org/10.1126/science.184.4139.865.

45. Olins, A.L., and Olins, D.E. (1974). Spheroid chromatin units (v bodies). Science *183*, 330–332. https://doi.org/10.1126/science.183.4122.330.

46. Reyes, A.A., Marcum, R.D., and He, Y. (2021). Structure and Function of Chromatin Remodelers. J. Mol. Biol. *433*, 166929. https://doi.org/10.1016/j.jmb.2021.166929.

47. Hao, F., Kale, S., Dimitrov, S., and Hayes, J.J. (2021). Unraveling linker histone interactions in nucleosomes. Curr. Opin. Struct. Biol. *71*, 87–93. https://doi.org/10.1016/j.sbi.2021.06.001.

48. Song, F., Chen, P., Sun, D., Wang, M., Dong, L., Liang, D., Xu, R.M., Zhu, P., and Li, G. (2014). Cryo-EM study of the chromatin fiber reveals a double helix twisted by tetranucleosomal units. Science *344*, 376–380. https://doi.org/10.1126/science.1251413.

49. Canzio, D., Larson, A., and Narlikar, G.J. (2014). Mechanisms of functional promiscuity by HP1 proteins. Trends Cell Biol. *24*, 377–386. https://doi.org/10.1016/j.tcb.2014.01.002.

50. Fussner, E., Strauss, M., Djuric, U., Li, R., Ahmed, K., Hart, M., Ellis, J., and Bazett-Jones, D.P. (2012). Open and closed domains in the mouse genome are configured as 10-nm chromatin fibres. EMBO Rep. *13*, 992–996. https://doi.org/10.1038/embor.2012.139.

51. Nishino, Y., Eltsov, M., Joti, Y., Ito, K., Takata, H., Takahashi, Y., Hihara, S., Frangakis, A.S., Imamoto, N., Ishikawa, T., and Maeshima, K. (2012). Human mitotic chromosomes consist predominantly of irregularly folded nucleosome fibres without a 30-nm chromatin structure. EMBO J. *31*, 1644–1653. https://doi.org/10.1038/emboj.2012.35.

52. Ou, H.D., Phan, S., Deerinck, T.J., Thor, A., Ellisman, M.H., and O'Shea, C.C. (2017). ChromEMT: Visualizing 3D chromatin structure and compaction in interphase and mitotic cells. Science *357*, eaag0025. https://doi.org/10.1126/science.aag0025.

53. Ayoub, N., Jeyasekharan, A.D., Bernal, J.A., and Venkitaraman, A.R. (2008). HP1-beta mobilization promotes chromatin changes that initiate the DNA damage response. Nature *453*, 682–686. https://doi.org/10.1038/nature06875.

54. Goodarzi, A.A., Noon, A.T., Deckbar, D., Ziv, Y., Shiloh, Y., Löbrich, M., and Jeggo, P.A. (2008). ATM signaling facilitates repair of DNA double-strand breaks associated with heterochromatin. Mol. Cell *31*, 167–177. https://doi.org/10.1016/j.molcel.2008.05.017.

55. Luijsterburg, M.S., Dinant, C., Lans, H., Stap, J., Wiernasz, E., Lagerwerf, S., Warmerdam, D.O., Lindh, M., Brink, M.C., Dobrucki, J.W., et al. (2009). Heterochromatin protein 1 is recruited to various types of DNA damage. J. Cell Biol. *185*, 577–586. https://doi.org/10.1083/jcb.200810035.

56. Sevilla, A., and Binda, O. (2014). Post-translational modifications of the histone variant H2AZ. Stem Cell Res. *12*, 289–295. https://doi.org/10.1016/j.scr.2013.11.004.

57. Smothers, J.F., and Henikoff, S. (2001). The hinge and chromo shadow domain impart distinct targeting of HP1-like proteins. Mol. Cell Biol. *21*, 2555–2569. https://doi.org/10.1128/MCB.21.7.2555-2569.2001.

58. Mendez, D.L., Kim, D., Chruszcz, M., Stephens, G.E., Minor, W., Khorasanizadeh, S., and Elgin, S.C.R. (2011). The HP1a disordered C terminus and chromo shadow domain cooperate to select target peptide partners. Chembiochem *12*, 1084–1096. https://doi.org/10.1002/cbic.201000598.

59. Vassallo, M.F., and Tanese, N. (2002). Isoform-specific interaction of HP1 with human TAFII130. Proc. Natl. Acad. Sci. USA *99*, 5919–5924. https://doi.org/10.1073/pnas.092025499.

60. Dyer, P.N., Edayathumangalam, R.S., White, C.L., Bao, Y., Chakravarthy, S., Muthurajan, U.M., and Luger, K. (2004). Reconstitution of nucleosome core particles from recombinant histones and DNA. Methods Enzymol. *375*, 23–44. https://doi.org/10.1016/s0076-6879(03)75002-2.

61. Schneider, C.A., Rasband, W.S., and Eliceiri, K.W. (2012). NIH Image to ImageJ: 25 years of image analysis. Nat. Methods *9*, 671–675. https://doi.org/10.1038/nmeth.2089.

62. Zivanov, J., Nakane, T., Forsberg, B.O., Kimanius, D., Hagen, W.J., Lindahl, E., and Scheres, S.H. (2018). New tools for automated high-resolution cryo-EM structure determination in RELION-3. Elife *7*, e42166. https://doi.org/10.7554/eLife.42166.

63. Pettersen, E.F., Goddard, T.D., Huang, C.C., Meng, E.C., Couch, G.S., Croll, T.I., Morris, J.H., and Ferrin, T.E. (2021). UCSF ChimeraX: Structure visualization for researchers, educators, and developers. Protein Sci. *30*, 70–82. https://doi.org/10.1002/pro.3943.

64. Simon, M.D., Chu, F., Racki, L.R., de la Cruz, C.C., Burlingame, A.L., Panning, B., Narlikar, G.J., and Shokat, K.M. (2007). The site-specific installation of methyl-lysine analogs into recombinant histones. Cell *128*, 1003–1012. https://doi.org/10.1016/j.cell.2006.12.041.

65. Philo, J.S. (2023). SEDNTERP: a calculation and database utility to aid interpretation of analytical ultracentrifugation and light scattering data. Eur. Biophys. J. *52*, 233–266. https://doi.org/10.1007/s00249-023-01629-0.

66. Ausio, J., Seger, D., and Eisenberg, H. (1984). Nucleosome core particle stability and conformational change. Effect of temperature, particle and NaCl concentrations, and crosslinking of histone H3 sulfhydryl groups. J. Mol. Biol. *176*, 77–104. https://doi.org/10.1016/0022-2836(84)90383-8.

67. Brown, P.H., and Schuck, P. (2006). Macromolecular size-and-shape distributions by sedimentation velocity analytical ultracentrifugation. Biophys. J. *90*, 4651–4661. https://doi.org/10.1529/biophysj.106.081372.

68. Schuck, P. (2000). Size-distribution analysis of macromolecules by sedimentation velocity ultracentrifugation and lamm equation modeling. Biophys. J. *78*, 1606–1619. https://doi.org/10.1016/S0006-3495(00)76713-0.

69. Kastner, B., Fischer, N., Golas, M.M., Sander, B., Dube, P., Boehringer, D., Hartmuth, K., Deckert, J., Hauer, F., Wolf, E., et al. (2008). GraFix: sample preparation for single-particle electron cryomicroscopy. Nat. Methods *5*, 53–55. https://doi.org/10.1038/nmeth1139.

70. Morin, A., Eisenbraun, B., Key, J., Sanschagrin, P.C., Timony, M.A., Ottaviano, M., and Sliz, P. (2013). Collaboration gets the most out of software. Elife *2*, e01456. https://doi.org/10.7554/eLife.01456.

71. Rohou, A., and Grigorieff, N. (2015). CTFFIND4: Fast and accurate defocus estimation from electron micrographs. J. Struct. Biol. *192*, 216–221. https://doi.org/10.1016/j.jsb.2015.08.008.

72. Bepler, T., Morin, A., Rapp, M., Brasch, J., Shapiro, L., Noble, A.J., and Berger, B. (2019). Positive-unlabeled convolutional neural networks for particle picking in cryo-electron micrographs. Nat. Methods *16*, 1153–1160. https://doi.org/10.1038/s41592-019-0575-8.

73. Punjani, A., Rubinstein, J.L., Fleet, D.J., and Brubaker, M.A. (2017). cryoSPARC: algorithms for rapid unsupervised cryo-EM structure determination. Nat. Methods *14*, 290–296. https://doi.org/10.1038/nmeth.4169.

74. Emsley, P., Lohkamp, B., Scott, W.G., and Cowtan, K. (2010). Features and development of Coot. Acta Crystallogr. D Biol. Crystallogr. *66*, 486–501. https://doi.org/10.1107/S0907444910007493.

75. Shekhar, M., Terashi, G., Gupta, C., Sarkar, D., Debussche, G., Sisco, N.J., Nguyen, J., Mondal, A., Vant, J., Fromme, P., et al. (2021). CryoFold: determining protein structures and data-guided ensembles from cryo-EM density maps. Matter *4*, 3195–3216. https://doi.org/10.1016/j.matt.2021.09.004.

76. Chi, H., Liu, C., Yang, H., Zeng, W.F., Wu, L., Zhou, W.J., Wang, R.M., Niu, X.N., Ding, Y.H., Zhang, Y., et al. (2018). Comprehensive identification of peptides in tandem mass spectra using an efficient open search engine. Nat. Biotechnol. *36*, 1059–1061. https://doi.org/10.1038/nbt.4236.

77. Chen, Z.L., Meng, J.M., Cao, Y., Yin, J.L., Fang, R.Q., Fan, S.B., Liu, C., Zeng, W.F., Ding, Y.H., Tan, D., et al. (2019). A high-speed search engine pLink 2 with systematic evaluation for proteome-scale identification of cross-linked peptides. Nat. Commun. *10*, 3404. https://doi.org/10.1038/s41467-019-11337-z.

STAR★METHODS

KEY RESOURCES TABLE

REAGENT or RESOURCE	SOURCE	IDENTIFIER
Bacterial and virus strains		
BL21 (DE3) *E. coli*	Thermo Scientific™	EC0114
BL21 (DE3) pLysS *E. coli*	Invitrogen	C602003
Dh5-alpha *E. coli*	Zymo Research	T3007
Chemicals, peptides, and recombinant proteins		
Histone H3 Kc9me3 C110A, Xenopus laevis	The Histone Source, Colorado State University	N/A
Histone H3 Kc9me3 C110A	This study	N/A
Histone H1.0, Human	NEB	M2501S
Histone H2A.Z, Mouse	This paper	N/A
Histone H2A, Xenopus laevis	This paper	N/A
Histone H2B, Xenopus laevis	This paper	N/A
Histone H4, Xenopus laevis	This paper	N/A
HP1α, Human	This paper	N/A
HP1αΔC, Human	This paper	N/A
Glutathione sepharose	Cytiva	17513201
Thrombin, bovine	Sigma-Aldrich	605157
Protease K	NEB	P8107S
ScaI	NEB	R3122L
MNase	Roche	10107921001
Critical commercial assays		
Q5 site-direct mutagenesis kit	NEB	E0554S
Deposited data		
Cryo-EM map of HP1α-H2A.Z nucleosome complex (map1)	This paper	EMD-42774
focused refined cryo-EM map of HP1α in complex with partial H2A.Z nucleosome (map2)	This paper	EMD-42690
focused refined cryo-EM map of K9me3_H2A.Z nucleosome (map3)	This paper	EMD-42692
Cryo-EM map of free K9me3_H2A.Z nucleosome	This paper	EMD-42773
coordinate of the HP1α-H2A.Z nucleosome complex	This paper	PDB: 8UXQ
Oligonucleotides		
H2AZ.1-LIC-F TTTAAGAAGGAGATATAGATCAT GGCTGGCGGTAAGGCTGG (IDT Integrated DNA Technologies, Inc.)	This paper	N/A
H2AZ.1-LIC-R TTATGGAGTTGGGATCTTATTAT CACACAGTCTTCTGTTGTCC (IDT Integrated DNA Technologies, Inc.)	This paper	N/A
GST HP1αΔC-F TAACTCGAGCGGCCGCATC GTGACTGACTG (IDT Integrated DNA Technologies, Inc.)	This paper	N/A
GST HP1αΔC-R TTCATAAAATGCTATCACAATTTGTGGAC (IDT Integrated DNA Technologies, Inc.)	This paper	N/A

(*Continued on next page*)

Continued

REAGENT or RESOURCE	SOURCE	IDENTIFIER
H3_K9C-F TGCTCCACCGGAGGGAAAGCTCCCCG (IDT Integrated DNA Technologies, Inc.)	This paper	N/A
H3_K9C-R GCGGGCGGTCTGCTTAGTACGAGCCAT (IDT Integrated DNA Technologies, Inc.)	This paper	N/A
H3_C110A-F CACCAACCTGGCCGCCATCCACG (IDT Integrated DNA Technologies, Inc.)	This paper	N/A
H3_C110A-R TCCTCAAACAAACCGACC (IDT Integrated DNA Technologies, Inc.)	This paper	N/A
Recombinant DNA		
Plasmid GST HP1α	Vassallo et al.[59]	Addgene 24074
Plasmid GST HP1αΔC	This paper	N/A
Plasmid 208-bp 601 Widom	Ed Luk	N/A
Plasmid mH2A.Z.1 in pIND-EGFP	Danny Rangasamy	Addgene 15770
Plasmid pET-LIC-mH2A.Z.1	This paper	N/A
Plasmid pET-H2A	Dyer[60]	N/A
Plasmid pET-H2B	Dyer[60]	N/A
Plasmid pET-H3	Dyer[60]	N/A
Plasmid pET-H4	Dyer[60]	N/A
Plasmid pET- H3_K9C_C110A	This paper	N/A
Software and algorithms		
ImageJ	Rasband et al.[61]	N/A
Prism5	GraphPad Software, Inc.	N/A
Relion	Zivanov et al.[62]	https://relion.readthedocs.io/en/release-4.0/
ChimeraX	Pettersen et al.[63]	https://www.cgl.ucsf.edu/chimerax/

EXPERIMENTAL MODEL AND STUDY PARTICIPANT DETAILS

The *E. coli*. strains used in this study are: BL21 (DE3) (Thermo Scientific), BL21 (DE3) pLysS (Invitrogen), and DH5-alpha (Zymo Research).

METHOD DETAILS

Expression and purification of HP1α

GST-tag human HP1α was a kind gift from Naoko Tanese (Addgene plasmid # 24074; http://n2t.net/addgene:24074 ; RRID:Addgene_24074). GST-tag HP1αΔC construct was generated by deleting amino acids #169 to 191 of the protein through site-direct mutagenesis. GST-HP1 and GST-HP1ΔC were expressed in BL21 (DE3) E. coli cells. Both proteins were purified using the same protocol as follows. Cells were lysed by sonication in buffer containing 50 mM Tris-HCl pH7.5, 400 mM NaCl, 10% glycerol supplemented with protease inhibitors and 1mM Dithiothreitol (DTT). Cell lysate was subjected to batched affinity chromatography purification using glutathione sepharose (Cytiva). HP1 proteins was released from the GST-tag by overnight thrombin digestion followed by purification on a 50HQ 10x100 column (Applied Biosystems) in a continuous gradient of 50 -1000 mM NaCl. Peak fractions were pooled and further purified by gel filtration with a Superdex 200 increase 10/300 GL column (GE Healthcare). Peak fractions were pooled and concentrated to 11 mg/ml.

Nucleosome reconstitutions

The plasmid with twelve tandem repeats of 208-bp 601 Widom sequence was a kind gift from Dr. Ed Luk. Large-scale plasmids were purified as previously described.[60] Restriction enzyme ScaI was used to excise the plasmids to generate single repeat of 208-bp segment. DNA fragments were further purified by polyethylene glycol precipitation and MonoQ anion exchange chromatography.

The sequence for the 208-bp Widom 601 DNA repeat is as follows:

ACTTATGTGATGGACCCTATACGCGGCCGCCCTGGAGAATCCCGGTGCCGAGGCCGCTCAATTGGTCGTAGACAGCTCTAGCAC CGCTTAAACGCACGTACGCGCTGTCCCCCGCGTTTTAACCGCCAAGGGGATTACTCCCTAGTCTCCAGGCACGTGTCAGATATAT ACATCCTGTGCATGTATTGAACAGCGACCTTGCCGGAGT.

Canonical *Xenopus* laevis histones H2B and H4 were expressed in BL21 (DE3) pLysS *E. coli* cells and purified as previously described.[60] Mouse H2A.Z.1 gene in pIND-EGFP was a kind gift from from Danny Rangasamy (Addgene plasmid # 15770 ; http://n2t.net/addgene:15770 ; RRID:Addgene_15770). It was re-cloned into pET-LIC expression vector. The protein was expressed in BL21 (DE3) *E. coli* cells and purified using the same procedure as the canonical histones. To produce histone H3 containing H3K9me3 mimic, a single point mutation K9C was first introduced on *Xenopus laevis* H3. A procedure to install a tri-methyl-Lysine analog (tri-MLA) on C9 was then performed as described.[64] Briefly, purified histone H3K9C was dissolved in Alkylation buffer (1M HEPES, 10 mM D/L-methionine, 4 M Guanidium-HCl, 20 mM DTT) and incubated for 1 hour at 37°C. 100 mg of (2-bromoethyl) trimethylammonium bromide was then added to the reaction mixture followed by incubation at 50°C for 2.5 hours. Afterward, DTT was added to a final concentration of 10 mM and the reaction mixture was further incubation at 50°C for another 2.5 hours. The reaction was quenched with 5 mM β-mercaptoethanol. The modified protein was separated and desalted using a PD-10 desalting column (GE Healthcare) that was pre-equilibrated in water supplemented with 2 mM β-mercaptoethanol. The final product was lyophilized and stored at -80°C. The presence of the H3K9me3 MLA was confirmed by mass spectrometry. For some nucleosome preparations, the same modified H3 was purchased from The Histone Source at Colorado State University.

Histone octamers containing the abovementioned histones were produced *in vitro* using salt dialysis as previously described.[60] Briefly, equal molar of each histone was mixed and incubated for 2 h in unfolding buffer (7 M guanidine HCl, 20 mM Tris, pH 7.5, and 10 mM DTT) followed by dialysis against at least three changes of refolding buffer (10 mM Tris, pH 7.5, 1 mM EDTA, pH 8.0, 2 M NaCl and 1 mM DTT) at 4°C. Octamer was concentrated and purified by gel filtration using a Superdex200 increase 10/300 GL column. Mono-nucleosomes were reconstituted by mixing the octamer with 208bp 601 Widom sequence DNA in equal molar ratio in high-salt buffer (10 mM Tris, pH 8.0, 2 mM EDTA, 2 M NaCl and 2 mM 2-Mercaptoethanol (βME) followed by overnight dialysis into low salt buffer (10 mM Tris, pH 8.0, 2 mM EDTA, 5 mM NaCl and 2 mM βME) as described.[60]

SV-AUC

SV-AUC studies were conducted in a Beckman XL-I using the absorption optics to scan cells assembled with a double sector charcoal EPON centerpiece and sapphire glass windows inserted into a AN-60 Ti rotor. All samples were exchanged into buffer containing 10 mM HEPES, 75 mM NaCl, and 0.5 mM TCEP at pH 7.5. The SV-AUC runs were conducted at 4°C and 48,000 rpm for HP1α and 38,000 for the HP1α-nucleosome complexes. For HP1α, samples with protein concentrations of 0.52, 1.82, and 4.15 μM were scanned at 230 nm. HP1α samples with protein concentrations of 3.38, 11.16 and 23.57 μM were scanned at 280 nm. The nucleosome and HP1α-nucleosome complex samples were scanned at the absorption maximum of DNA, 260 nm. Nucleosome at a constant concentration of 0.16 μM was titrated with increasing concentrations of HP1α ranging from 0.1 to 23.73 μM. The data point at 0.01μM is nucleosome without added HP1α.

A value of $\bar{\nu} = 0.7282$ was calculated from the sequence of HP1α using the program SEDNTERP.[65] A measured value of $\bar{\nu} = 0.65$ for a nucleosome was used to analyze the HP1α-nucleosome complexes.[66] The sedimentation parameters were corrected to S(20,w) using values of $\rho = 1.00393$ and $\eta = 1.5926$ at 4°C calculated with Sedenterp from the buffer composition. Continuous distribution component analysis, c(s), was conducted using the program Sedfit[67,68] to deconvolute the species present in a solution. The software Prism version 10.0.1 was used to plot the c(s) distributions and the dependence of S(20,w) on HP1α and HP1α-nucleosome complex concentration. The HP1α-nucleosome titration was fit to the Hill equation with a function that explicitly calculates the free concentration of the HP1α ligand.

MNase assays

For the digestion assay with MNase, 340 nM nucleosome was subjected to digestion with 0.75U of MNase (Roche) in a 65 μl reaction in MNase buffer (10 mM Tris pH7.4, 50 mM NaCl, 2 mM $CaCl_2$) in the presence of 4-fold excess of HP1α at 37°C. For experiments containing linker histone H1.0 (NEB # M2501S), 1:1 ratio of H1:nucleosome was used. Nucleosomes with or without HP1α and/or H1.0 were mixed and incubated for 30min prior to MNase digestion. Samples (4.5 μl) were collected every 3 min. 8 μl stop/deproteinization buffer (10 mM Tris–HCl, pH 8.0, 0.6% SDS, 40 mM EDTA, 0.1 mg/ml proteinase K) was added to quench the reaction followed by 1 hour incubation at 55°C. The samples were resolved on 8% (19:1 Acrylamide/Bis) Native-PAGE (at 100V, 120 min). The gel was stained with SYBR-Gold and imaged with Typhoon imager (Cytiva). Images were analyzed using ImageJ software. Intensities for fragments with sizes of 180-200, 160, 140, and 100 bp were calculated. Two-way Anova test was used to determine the level of significant difference ($p \leq 0.05$). Two-way Anova test and graphical representation was done using Prism 5 software.

Nucleosome binding assay

HP1α and HP1α**Δ**C was dialyzed for 3 hours in binding buffer (10 mM Tris, pH 8. 25 mM NaCl, 2 mM EDTA, 1 mM DDT) separately prior to nucleosome binding reaction. 250 nM nucleosomes (containing $H3K9_cme3$ or $H2A.Z\text{-}H3K9_cme3$) in a final volume of 15 μl were mixed with increasing amount of HP1α. The mixture was incubated on ice for 30 min. The reactions were then resolved on 4% Native-PAGE (100 V, 90 min) and stained with SYBR-Gold before imaging by FluorChem8900 Imager (Alpha Innotech).

Assembly of the HP1α-H2A.Z-H3K9$_c$me3 nucleosome complex for cryo-EM study

Three Gradient Fixation (GraFix) experiments with three different protein preparations were conducted to produce the samples used for the cryo-EM study. In two Grafix experiments 1.2 μM of nucleosome was mixed with 75-fold excess of HP1α (90 μM) in 500 μl reaction in binding buffer A (10 mM Tris, pH 8. 25 mM NaCl, 2 mM EDTA, 1mM DDT). In the third experiment, similar condition was applied except that 32-fold excess of HP1α (38.4 μM) and buffer containing 75 mM NaCl were used. In each experiment, HP1α-nucleosomes mixture was incubated on ice for 30 min and then concentrated to 200ul before subjected to GraFix[69] for separation and cross-linking. The continuous density gradient was formed by mixing two buffer solutions with a Gradient Master (BioComp). The top buffer contains 10 mM HEPES, 20 mM NaCl, 1mM DTT and 5% sucrose, while the bottom buffer contains 10 mM HEPES, 20 mM NaCl, 1 mM DTT, 25% sucrose and 0.2% glutaraldehyde. Ultracentrifugation was carried out at 4°C in a SW41 rotor (Beckmann) for 16 hours with speeds of 27,000 rpm. Following centrifugation, the gradients are fractionated. The optical density of each fraction was measured with a Nanodrop Spectrophotometer (Thermo Fisher). Peak fractions were further examined by Native-PAGE gels and by negative-stained EM to identify the complex. Complex formation was observed in all three experiments, within a similar pattern of complex separation from free nucleosomes. Fractions containing the complex were pooled, dialyzed into storage buffer (10 mM HEPES pH 8, 20 mM NaCl, 1 mM DTT) and concentrated to 2-3.8 μM.

Cryo-EM sample vitrification

Cryo-EM grids were prepared using Vitrobot Mark IV (FEI Company) under 8°C and 100% humidity. Aliquots of 3.5 μl of the HP1α-H2A.Z nucleosome complex or the free K9me3-H2A.Z nucleosome were applied to glow-discharged QUANTIFOIL grids (R1.2/1.3 – 400 mesh), blotted for 4 to 5 seconds and plunged into liquid ethane cooled by liquid nitrogen. Grids were stored in liquid nitrogen until they were imaged.

Cryo-EM data collection

Grid screening was done using the Talos Arctica microscope (FEI) at the cryo-EM facility in Stony Brook University to identify suitable grids for data collection. For the HP1α-nucleosome samples, multiple datasets were collected at the University of Virginia Molecular Electron Microscopy Core using the Titan Krios electron microscope (FEI Company) operating at 300 kV with a nominal magnification of 81,000X, giving a pixel size of 1.08 Å at the specimen level. Movies were recorded using a K3 direct detector (Gatan company) in counting mode using EPU software, with the Bioquantum energy filter operating at zero loss frequency 10 eV. Defocus values range from -1.0 to -2.25 μm. Each movie was dose-fractionated to 40 frames with a dose rate of ∼1.25 e/Å^2/sec. Total dose per micrograph is 50 e/ Å^2 (Table S1).

For the K9me3-H2A.Z nucleosome sample, one dataset was collected at the Laboratory of Biomolecular Structure at Brookhaven National Laboratory (BNL) using the Titan Krios electron microscope (FEI Company) operating at 300 kV with a nominal magnification of 105,000X giving a pixel size of 0.825 Å at the specimen level. Movies were recorded using a K3 direct detector (Gatan company) in counting mode using EPU software, with the Bioquantum energy filter operating at zero loss frequency 15 eV. Defocus values range from -1.0 to -2.5 μm. Each movie was dose-fractionated to 40 frames with total dose per micrograph being 40 e/ Å^2 (Table S1).

Image analysis

Software for image analysis were administered by SBGrid consortium.[70] For the HP1α-nucleosome datasets, frames were aligned and summed using the motion correction software implemented within RELION.[62] The CTF parameters were estimated using CTFFIND4.[71] Particle-picking was carried out using Topaz neural-network picking.[72] Both particle-picking and 2D classification were done in cryoSPARC,[73] while the rest of image processing steps were carried out in RELION. Specifically, bad particles were removed through multiple rounds of 2D classifications, resulting in a data set of 1.3-millions of particles, which were then subjected to 3D classification in RELION. Good 2D classes representing different views of the complex were selected and used for the Ab-Initio reconstruction in cryoSPARC. The subsequent low-resolution map was used as the initial model for 3D classification in RELION. After three rounds of 3D classifications, the best class containing 74,257 particles was selected and subjected to consensus 3D refinement. The particles were then subjected to Bayesian Polishing and postprocessing, yielding map with an average resolution of 4.1 Å. The global resolution of the map was estimated using the gold standard Fourier Shell Correlation (FSC) 0.143 criterion with automatic B factor determined in RELION. Local resolution was estimated in RELION.

To improve the resolution of the HP1 region, we performed signal subtraction and focused refinement in RELION. Briefly, the consensus map was used to generate two overlapping masks using the Volume eraser tool in UCSF ChimeraX.[63] One mask contains only the nucleosome region, while the second mask contains HP1 density and most of the nucleosome (mask 2 and mask 3 in Figure S2C). Multibody refinement was then performed using these two masks. The subsequent volumes representing the two body were used as new masks to perform signal subtraction and focus-refinement, which resulted in improved resolution and map feature of the two bodies.

Image processing of the H2A.Z-H3K9$_c$me3-nucleosome dataset was performed using cryoSPARC.[73] Briefly, a dataset containing 454,841 particles were generated after Topaz neural-network particle picking followed by two-rounds of 2D classification. This dataset was then subjected to additional rounds of 3D heterogeneous refinement, which resulted in a final subset of 186,172 particles. Non-uniform refinement was performed with this subset to generate the final map (Figure S5).

All conversions between RELION and CryoSPARC were performed using D. Asarnow's pyem script (personal communication; https://github.com/asarnow/pyem). The generation of figures featuring images related to the structural model was carried out using UCSF ChimeraX and Coot.[74] Movies were created using UCSF ChimeraX.

Model building and refinement

The specific refinement protocol applied to the HP1 model involves iteratively applying Cascade Molecular Dynamics Flexible Fitting (cMDFF),[27] Modelling Employing Limited Data (MELD),[28] and Molecular Dynamics Flexible Fitting (MDFF)[27] to optimize the atomic coordinates of the model to match the experimental density map obtained through Cryo-EM (Figure S3). This process is described in more detail below. The cross-correlation coefficient, a commonly used metric in the field of structural biology, is employed as a measure of the similarity between the experimental density map and the atomic model. This metric is used to evaluate the quality of the refined model.

To generate an initial model for refinement, a modified H2A.Z nucleosome coordinate (combining the histone octamer of PDB: 1F66 with the Widom 601 DNA from PDB: 6FQ5) and the Alphafold model of full-length human HP1α (AF-P45973) was used. The H2A.Z nucleosome placement was determined by rigid-body fitting using UCSF ChimeraX.[63] For HP1α, we extracted the different domains as individual molecules and used ChimeraX to perform rigid-body docking to determine their initial placements. The initial positions of the two CDs and the CSD-CSD dimer were determined by docking these molecules separately in the focused refined map of the HP1α-nucleosome complex (map 2 in Figure S3). The flexible regions of NTE, HR, and CSD were excluded during initial model building. Some visible secondary structures and prior knowledge of the CSD-CSD dimerization (Figure S3D) were used to guide the initial model building. We kept the overall configuration of the two CSDs in a similar dimer conformation observed in the crystal structures of Drosophila CSD-CSD dimers.[34] The CSD-CSD dimer configuration were preserved during the manual rigid-body fitting. The positions of the two CD2 can be unambiguously determined. While the orientation of the CSD-CSD dimer relative to the nucleosome can be determined, its precise configuration is less clear due to the limited resolution of the map at the HP1-nucleosome interface.

Once the optimal placements of the CDs and CSD-CSD domains were identified, the flexible loops (NTE, HR and CTE) were added and reconnected to form a full-length HP1α. The reconnection was done using VMD's psfgen tool which takes in the necessary topology files and generates the appropriate structure files. Specifically, patches were applied between the CD / CSD domains and the respective NTE, HR, and CTE domains followed by minimization to alleviate nonphysical bonds and structural features. This process yielded an initial structure of the HP1 dimer-H2A.Z nucleosome complex (Figure S3B).

Equilibrium MD

The initial model was then subjected to a minimization and 50 ns equilibration simulation using GPU-accelerated NAMD3 software, implementing CHARMM36 force fields and a TIP3 water model parameterization for the protein / nucleic and solvent components.

MDFF/cMDFF

The subsequent equilibrated structure was fitted to a series of four density maps each with increased resolution using the cMDFF protocol (Figure S3B). The maps were created by smoothing the original density map, obtained from Cryo-EM data, by applying a Gaussian blur with a half-width parameter σ. The first map applied a Gaussian blur with $\sigma = 6$ Å; each subsequent map was smoothed by 2 Å less than the previous map until the final map which corresponded to the original Cryo-EM map resolution. Each MDFF fitting simulation was run for 50 ns using NAMD3 software and CHARMM36 force fields and was restricted to the backbone atoms. The fit of the model was evaluated using VMD timeline analysis, where a cross-correlation coefficient (CCC) was calculated at each time step along the trajectory to measure the degree of fitness of the model with respect to the density of interest.

MELD

The MELD protocol was integrated into the computational workflow in conjunction with cMDFF and MDFF, as illustrated in (Figures S3A and S3B). This design is an extension of the CryoFold algorithm, a multiphysics approach that generates equilibrium ensembles of biomolecular structures from cryo-EM data,[75] leading to a comprehensive sampling of the conformational landscape of the complex. The incorporation of MELD allowed for the implementation of precise restraint applications, which are not feasible using standard restrained MD methods. These restraints were applied as flat-bottom harmonic potentials, and their satisfaction resulted in no additional contribution to the energy function, i.e., they fell within the flat-bottom region. However, for restrictions that fell outside this region, energy penalties were applied, which acted as a redirecting force guiding the system towards low-energy basins.

The MELD simulations used a Replica Exchange Molecular Dynamics (REMD) sampling method with a 16-replica parameterization, a temperature range of 300-380K, a GBNeck2 implicit solvent model, and a simulation time of 250 ns. A linear temperature ramp was applied throughout the one-dimensional Hamiltonian exchange ladder starting from replica 1 and finishing at replica 6. Additionally, distance restraints were applied linearly throughout the ladder starting at replica 7 and finishing at replica 16 with a force constant of 250 kJ / (mol * nm2). Specifically, cartesian restraints were enforced in regions with a high map correlation determined from earlier cMDFF results. These regions were assigned confidence values of 100% in each and every replica (1-16). Distance restraints between alpha carbons were applied throughout the remaining domains starting at replica 7 and finishing at replica 16. These restraints were applied with varying confidence values ranging from 50-90% based on external experimental information. This approach resulted in an ensemble of the lowest free energy structures consistent with experimental knowledge. The bsc1 and ff14SB forcefields in AMBER were used to generate the appropriate topology and parameter file for MELD simulations.

These procedures resulted in a marked improvement in the CCC, however, certain regions, particularly flexible loop regions throughout the model remained positionally ambiguous, necessitating further refinement and sampling of the conformational space.

To preserve the accuracy of the mapping obtained from cMDFF, high-energy Cartesian restraints were applied to the alpha carbons in regions that displayed high map correlation from cMDFF. These restraints penalized any deviation of more than 0.2 nm from the initial Cartesian coordinates, thus restricting their deviation from the initial positions. Additionally, the restraints were lifted from flexible loop regions to optimize the exploration of the conformational space, reflecting the likelihood function utilized throughout the MELD simulations. The constrains applied to different regions of the complex were indicated in Figure S3C. MELD simulations reveal various conformations of the flexible loop regions, notably the H3 tail (Figure S3B), that better fit the density.

XL-MS and data analysis

Bissulfosuccinimidyl suberate (BS3) Crosslink test was performed to test and analyze stable amide bonds. K9me3-H2A.Z nucleosomes (2.44 μM) and 4-fold access of purified recombinant human HP1α (9.76 μM) were mixed in a final volume of 50 μl reaction and dialyzed into binding buffer [75 mM NaCl, 10 mM HEPES, 0.4 mM 2-Mercaptoethanol and 1 mM DTT] at 4°C for 3 hours. Then, fresh 2 mM DTT was added. BS3 crosslinker (250 μM and 1 mM respectively) was added to the HP1α control and the HP1α-nucleosome complex and the reactions were incubated at 25°C for 45 minutes. After the incubation, samples were quenched with 50 mM Tris-HCl pH7.5 for 15 minutes at room temperature. The samples were flash frozen in liquid nitrogen then stored in -80°C freezer until XL-MS analysis.

Frozen samples were thawed and were separated using SDS-PAGE (200 V, Thermo Fisher NP0050, NP0335BOX) and stained with GelCode Blue (Thermo Fisher 24592). Supershifted bands were excised from the gel, destained twice with 100-fold (m/m) excess of 50% acetonitrile (ACN, Millipore Sigma 900667) in 25 mM LC-MS-grade ammonium bicarbonate (ABC, Honeywell Fluka, 40867), 37^0C, 30 min, with agitation. Destained slices were replaced into 100 μl of 50 mM tris-2-carboxyethyl) phosphine (TCEP, Millipore Sigma, 646547), incubated for 10 min at 60°C, and destained as described above. Destained sliced were incubated in 100% ACN, and air dried for 10 min, before addition of 75 μl of 25 mM ABC, supplemented with 50 ng/μl of MS-grade trypsin (Thermo Fisher 90305) and 0.01% ProteaseMAX Surfactant (Promega, V2071). Digestion was carried out for 120 min at 54^0C, peptides were collected as described in ProteaseMax application note (Promega, TB373, Rev. 2/15), and purified using Pierce C18 Spin Tips (Thermo Fisher PI84850). Peptide samples were dissolved in 0.1% (v/v) formic acid (FA, Thermo Fisher Scientific, LS118-4) for MS analysis. Peptides were analyzed in an Orbitrap Fusion Lumos mass spectrometer (Thermo Scientific) coupled to an EASY-nLC (Thermo Scientific) liquid chromatography system, with a 2 μm, 500 mm EASY-Spray column (Thermo Scientific, ES903). The peptides were loaded on the column in 100% buffer A (0.1% FA in water), and eluted at 200 nl/min over either linear 140 min gradient 4-40% buffer B (0.1 % FA in ACN, Thermo Scientific 85174), or 195 min concave gradient (4-30%, curve value set at 6). Each full MS scan (R = 60,000) was followed by 20 data-dependent MS2 (R = 15,000) with high-energy collisional dissociation and an isolation window of 2.0 m/z. The normalized collision energy was set to 30%. Notable selection algebra included 4-6 charge precursor isolation window, TopN, [lowest charge then most intense] operators. Monoisotopic precursor selection was enabled and the dynamic exclusion window was set to 30.0 s. Resulting raw files were searched in enumerative and cross-link discovery modes. Enumerative mode was engaged by applying open search implemented in the pFind3 software[76] using the fasta file combining sequences of the recombinant targets and the expression host proteome (*E. coli*, Uniprot UP000000625) as the search space. Fasta sequences of proteins identified in the samples in the enumerative mode were combined to form the search space for crosslink discovery by pLink2[77]; protein modifications inferred by pFind3 and comprising >0.5% of the total were included as the variable modifications in pLink2 search parameters. pLink2 results were filtered for FDR (<5%), e-value (<1.0E-3), score (<1.0E-2).

QUANTIFICATION AND STATISTICAL ANALYSIS

In Figures 6B–6D, the average values of three biological replicas were shown with the standard deviation of the mean (SD) in each case. In all cases, reproducible results were obtained.